THE VALIDITY OF THE CONTINUUM LIMIT IN THE SMOOTH POTENTIAL DESCRIPTION OF N-BODY SYSTEMS

By

IOANNIS V. SIDERIS

A DISSERTATION PRESENTED TO THE GRADUATE SCHOOL
OF THE UNIVERSITY OF FLORIDA IN PARTIAL FULFILLMENT
OF THE REQUIREMENTS FOR THE DEGREE OF
DOCTOR OF PHILOSOPHY

UNIVERSITY OF FLORIDA

2002

Copyright 2002

by

Ioannis V. Sideris

To the memory of Professor Heinrich Eichhorn.

ACKNOWLEDGMENTS

I believe this page is always a very small space to express any acknowledgment that is truely and deeply felt. And this is because it is so difficult to express formally the informal, to put in fancy words the meaning, importance and complexity of the everyday interaction that can contribute or even build from base zero ideas and perspectives.

I feel that only very few people honestly appreciated or understood my work. This is not necessarily bad, it is rather interesting and it raises questions. In this travel I had the great luck to be guided by Professor Henry E. Kandrup, the person who believed in me when everybody else (including me) seemed to have lost faith. His help was so big, and so important that I doubt if it is possible to be expressed by letters, words, and paragraphs. Typical symbols of communication of the ordinary life were never adequate to describe the extraordinary. Professor Kandrup did not only teach me the practical issues or techniques of how to be a good scientist, He taught me how to think as a scientist, how to trust my intuition, how to develop my ideas, and how to always try to see things from a new perspective. Is n't "the different perspective" really the basis of not simply science but of the progress in science? But Dr. Kandrup also gave me something more important: He gave me his friendship, and several hundreds hours of coffee breaks, enriched with wisdom, interaction of ideas, ocassional fights, but surely many more laughs. Only now I realise how important these coffee breaks were to me, and how deeply they shaped my way of thinking. Who we are is always built in the most unsuspicious times. A big thank you Henry, I will miss all this.

I also have to thank some more people who helped and guided me. Firstly Professor Heinrich Eichhorn who was the very first person to believe in me. He opened the way, and I am sure he smiles now from wherever he is, because he knows that he was right about "the salt and pepper of science." I would also like to thank Professor Courtland Bohn, for his help and support. Also the members of my committee, Dr. Dufty, Dr. Hunter, Dr. Smith, Dr. Pop-Stojanovic, and Dr. Ipser who were very friendly and supportive when I asked for their help. I would also like to thank my family for all their support. Also a big "thank you" to Gaby: it was a very long journey but you were always there for me. And finally all my friends who stood by me through the good but most importanly through the bad, difficult times. In this world lucky are the ones who have good friends.

TABLE OF CONTENTS

page

ACKNOWLEDGMENTS iv

LIST OF FIGURES viii

ABSTRACT xii

CHAPTERS

1 INTRODUCTION 1

2 MATHEMATICAL FORMULAS 10

2.1 Plummer Potential 10
2.2 Three-dimensional harmonic oscillator 11
2.3 Three-dimensional harmonic oscillator plus a perturbation factor 11
2.4 A triaxial generalisation of Dehnen potential 12

3 INTEGRABLE POTENTIALS 14

3.1 Divergence Laws 14
3.2 Average Short-time Lyapunov Exponents 23
3.3 Power Spectra and Complexities 26

4 NONINTEGRABLE POTENTIALS 31

4.1 Divergence Laws 31
4.2 Average Short-time Lyapunov Exponents 33
4.3 Power Spectra and Complexities 35
4.4 Transitions Between Regular and Chaotic Behaviour 35

5 CHAOTIC MIXING 39

6 LANGEVIN DESCRIPTION 46

7 NUMERICAL ESTIMATION OF SMOOTH LYAPUNOV EXPONENTS 53

8 CONCLUSIONS 57

REFERENCES 62

BIOGRAPHICAL SKETCH 65

LIST OF FIGURES

Figure page

3.1 (a) The deviation $\Delta r = |\mathbf{r}-\mathbf{r}_s|$ from the smooth potential characteristic for one representative frozen-N orbit evolved with $\epsilon = 10^{-4}$ and $N = 10^3$. (b) Another frozen-N orbit evolved with the same ϵ and N for the same initial condition. (c) and (d) the same for $N = 10^5$. 16

3.2 (a) The quantity $\Delta r/\sqrt{2R_s^2}$ for frozen-N simulations with $N = 10^3$ and $\epsilon = 10^{-4}$. (b) The same data subjected to boxcar averaging over an interval $t = t_D$. (c) and (d) The same for $N = 10^5$. 19

3.3 Best fit values of the time scale $t_G(N)$ associated with the divergence of smooth and frozen-N orbits for two different initial conditions: $\Delta r/R_s = \Delta v/V_s \equiv t/t_G$. The dashed line has slope 1/2, corresponding to an $N^{1/2}$ dependence. 20

3.4 Best fit values of the time scale $t_J(N)$ associated with changes in angular momentum for frozen-N orbits for two different initial conditions: $\Delta J^2/J_s^2 \equiv t/t_J$. The dashed line has slope 1/2, corresponding to an $N^{1/2}$ dependence. 22

3.5 Mean short-time Lyapunov exponent $\langle\chi\rangle$ as a function of softening parameter ϵ for $N = 10^5$ (solid line), $N = 10^{4.5}$ (dotted), $N = 10^4$ (dashed), $N = 10^{3.5}$ (dot-dashed), $N = 10^{3.0}$ (triple-dot dashed), and $N = 10^{2.5}$ (broad dashed). The integrations were all performed for a single 'typical' initial condition. 24

3.6 Mean short-time Lyapunov exponent $\langle\chi\rangle$ as a function of particle number N for $\epsilon = 10^{-5}$ (solid line), $\epsilon = 10^{-4}$ (dotted), $\epsilon = 10^{-3}$ (thin-dashed), $\epsilon = 10^{-2}$ (dot-dashed), and $\epsilon = 10^{-1}$ (triple-dot dashed), all computed for the initial condition used to generate Figure 3.5. The short-time $\langle\chi\rangle$ for a different initial condition corresponding to a smooth radial orbit, again evolved with $\epsilon = 10^{-5}$, is indicated by the curve with thick dashes. 25

3.7 The x-y projection of representative frozen-N orbits generated from the same initial condition, evolved for $t = 25t_D$ with $\epsilon = 10^{-5}$. (a) $N = 10^{2.5}$. (b) $N = 10^3$. (c) $N = 10^{3.5}$. (d) $N = 10^4$. (e) $N = 10^{4.5}$. (f) $N = 10^5$. (g) $N = 10^{5.5}$. (h) The x-y projection of the same initial condition evolved in the smooth potential. 28

3.8 (a) The Fourier transformed $|x(\omega)|$ for one frozen-N integration of the initial condition used to generate Figure 3.7, evolved with $\epsilon = 10^{-5}$ and $N = 10^{2.5}$. (b) The same for $N = 10^3$. (c) $N = 10^{3.5}$. (d) $N = 10^4$. (e) $N = 10^{4.5}$. (f) $N = 10^5$. (g) $N = 10^{5.5}$. (h) $|x(\omega)|$ for a characteristic in the smooth potential with the same initial condition, with data recorded at the same intervals for the same total integration time. 29

3.9 Two probes of the complexity of frozen-N orbits for an ensemble of orbits with the same initial condition evolved with $\epsilon = 10^{-5}$. The solid curve exhibits $f_{0.1}$, the number of frequencies which have power equal to at least 10% of the power in the peak frequencies. The dashed curve exhibits $k_{0.95}$, the number of frequencies required to capture 95% of the total power. The vertical lines show $f_{0.1}$ and $k_{0.95}$ for a smooth characteristic generated identically from the same initial condition, thus exhibiting the intrinsic limitations associated with the discrete time series of data points. 30

4.1 The mean separation, Dr, between frozen-N orbits and smooth characteristics with the same initial conditions, computed for ensembles of 800 chaotic initial conditions evolved in the potential (2.6) for variable N. (a) $N = 10^{2.5}$. (b) $N = 10^3$. (c) $N = 10^{3.5}$. (d) $N = 10^4$. (e) $N = 10^{4.5}$. (f) $N = 10^5$. (g) $N = 10^{5.5}$. (h) The growth rate $t_G(N)$ extracted from the preceding panels, assuming a linear growth law. The solid line overlays a least squares fit $t_G = A + B \log_{10} N$. 32

4.2 Estimates of the largest Lyapunov exponent for orbits evolved in frozen-N realisations of a homogeneous ellipsoid: integrable initial conditions evolved with $M_{BH} = 0$ (solid line), 'sticky' initial conditions evolved with $M_{BH} = 10^{-1.5}$ (dashed line), and 'wildly chaotic' initial conditions with $M_{BH} = 10^{-1.5}$ (dot-dashed line). 34

4.3 The quantity Dr for two different initially localised ensembles of 'sticky' chaotic orbits with the same (low) energies, each evolved in frozen-N realisations of the Dehnen potential. (a) A 'regular' ensemble with $N = 10^4$. (b) A 'chaotic' ensemble with $N = 10^4$. (c) The 'regular' ensemble with $N = 10^{4.5}$. (d) The 'chaotic' ensemble with $N = 10^{4.5}$. (a) The 'regular' ensemble with $N = 10^5$. (b) The 'chaotic' ensemble with $N = 10^5$. 36

4.4 The mean Lyapunov exponent $\langle \chi_S \rangle$, for ensembles evolved in the smooth Dehnen potential, selecting as initial conditions the final phase space coordinates of orbits that had been evolved in frozen-N potentials for some time τ. (a) Initially regular (solid line) and chaotic (dashed line) low energy orbits evolved with $N = 10^4$. (b) Initially regular (solid line) and chaotic (dashed line) higher energy orbits evolved with $N = 10^4$. (c) The same as (a) but for $N = 10^{4.5}$. (d) The same as (b) but for $N = 10^{4.5}$. (e) The same as (a) but for $N = 10^5$. (f) The same as (b) but for $N = 10^5$. 37

5.1 The configuration dispersion σ_τ associated with an initially localised ensemble evolved in frozen-N realisations of the integrable ellipsoid potential (2.5) for variable N. (a) $N = 10^{2.5}$. (b) $N = 10^3$. (c) $N = 10^{3.5}$. (d) $N = 10^4$. (e) $N = 10^{4.5}$. (f) $N = 10^5$. 40

5.2 The configuration dispersion σ_τ associated with an initially localised ensemble evolved in frozen-N realisations of the integrable Plummer potential (2.2) for variable N. (a) $N = 10^3$. (b) $N = 10^{3.5}$. (c) $N = 10^4$. (d) $N = 10^{4.5}$. (e) $N = 10^5$. (f) Evolution in the smooth potential. 42

5.3 The configuration dispersion σ_τ associated with an initially localised ensemble of wildly chaotic orbits evolved in frozen-N realisations of the nonintegrable potential (2.6) for variable N. (a) $N = 10^{2.5}$. (b) $N = 10^3$. (c) $N = 10^{3.5}$. (d) $N = 10^4$. (e) $N = 10^{4.5}$. (f) $N = 10^5$. (g) $N = 10^{5.5}$. (h) Evolution in the smooth potential. . . 43

5.4 The configuration dispersion σ_τ associated with an initially localised ensemble of 'sticky' chaotic orbits evolved in frozen-N realisations of the nonintegrable potential (2.6) for variable N. (a) $N = 10^{2.5}$. (b) $N = 10^3$. (c) $N = 10^{3.5}$. (d) $N = 10^4$. (e) $N = 10^{4.5}$. (f) $N = 10^5$. (g) $N = 10^{5.5}$. (h) Evolution in the smooth potential. . . 44

6.1 The configuration dispersion σ_τ associated with an initially localised ensemble evolved in the smooth Plummer potential (2.2), perturbed by noise with $\Theta = 1.0$ and variable η. (a) $\eta = 10^{-3}$. (b) $\eta = 10^{-3.5}$. (c) $\eta = 10^{-4}$. (d) $\eta = 10^{-4.5}$. (e) $\eta = 10^{-5}$. (f) $\eta = 10^{-5.5}$. 48

6.2 The configuration dispersion σ_τ associated with an initially localised ensemble of wildly chaotic orbits evolved in the presence of noise of the nonintegrable ellipsoid potential (2.4) for $\Theta = 1.0$ and variable η. (a) $\eta = 10^{-2.0}$. (b) $\eta = 10^{-2.5}$. (c) $\eta = 10^{-3.0}$. (d) $\eta = 10^{-3.5}$. (e) $\eta = 10^{-4.0}$. (f) $\eta = 10^{-4.5}$.(g) $\eta = 10^{-5.0}$. (h) $\eta = 10^{-7.5}$. 49

6.3 The configuration dispersion σ_r associated with an initially localised ensemble of 'sticky' chaotic orbits evolved in the presence of noise of the nonintegrable ellipsoid potential (2.4) for $\Theta = 1.0$ and variable η. (a) $\eta = 10^{-2.0}$. (b) $\eta = 10^{-2.5}$. (c) $\eta = 10^{-3.0}$. (d) $\eta = 10^{-3.5}$. (e) $\eta = 10^{-4.0}$. (f) $\eta = 10^{-4.5}$. (g) $\eta = 10^{-5.0}$. (h) $\eta = 10^{-7.5}$. 50

6.4 The mean complexity n for orbits evolved in the potentials (2.3), (2.1), and (2.6), considering both frozen-N orbits with variable N (diamonds) and smooth orbits perturbed by noise with $\Theta = 1.0$ and variable η (triangles). η was related to N by the relation $\eta = e^{\mathcal{A}}/N$, with $\mathcal{A}$ determined as described in the text. The dashed horizontal line exhibits the mean complexity of orbits with the same initial conditions evolved in the smooth potential in the absence of noise. (a) Regular orbits in the Plummer potential. (b) Regular orbits in the three-dimensional harmonic oscillator potential. (c) Wildly chaotic orbits in the three-dimensional harmonic oscillator plus perturbation potential. (d) 'Sticky' chaotic orbits in the ellipsoid plus black hole potential. 52

7.1 The mean spatial separation between orbits generated in the frozen-N analogue of the Plummer potential, from initial conditions seperated in configuration space by a distance $\delta r(0) = 10^{-5}$. The four curves correspond (from top to bottom) to $N = 10^{4.5}$, $N = 10^5$, $N = 10^{5.5}$, $N = 10^6$. Each curve was generated by averaging over 100 pairs of initial conditions. 55

7.2 The mean spatial separation between orbits generated in the frozen-N analogue of the three-dimensional plus perturbation potential, from initial conditions seperated in configuration space by a distance $\delta r(0) = 10^{-5}$. The four curves correspond (from top to bottom) to $N = 10^{4.5}$, $N = 10^5$, $N = 10^{5.5}$, $N = 10^6$. The solid curve corresponds to a slope of 0.022, generated as a least squares fit. The triple dot-dashed line has a slope 0.026, equal to the mean value of the smooth Lyapunov exponent. The dashed line has a slope 0.75, equal to the mean value of the N-body Lyapunov exponent χ_N. Each curve was generated by averaging over 100 pairs of initial conditions. 56

Abstract of Dissertation Presented to the Graduate School
of the University of Florida in Partial Fulfillment of the
Requirements for the Degree of Doctor of Philosophy

THE VALIDITY OF THE CONTINUUM LIMIT IN THE SMOOTH POTENTIAL DESCRIPTION OF N-BODY SYSTEMS

By

Ioannis V. Sideris

August 2002

Chair: Henry E. Kandrup
Major Department: Astronomy

This thesis attempts to give quantitative as well as qualitative answers to the question of the validity of the continuum limit as an analogue to N-body systems. A number of simulations were performed in both integrable and nonintegrable smooth potentials and their frozen-N analogues and comparisons were made using a number of quantitative tools. The comparisons took place on both statistical and pointwise levels. Also useful measures associated to nonlinear dynamics were used. The results of this study suggest that there is always microscopic chaos present in the N-body configurations that is associated with discreteness effects. This chaos is different from the macroscopic chaos which may be associated with the bulk potential and persists even for very large N. Therefore the Lyapunov exponents of orbits evolving in N-body environments do not decrease as N increases. However

pointwise comparisons associated with the power spectra of the orbits as well as their statistical properties suggest that the continuum limit does make sense.

CHAPTER 1
INTRODUCTION

Galaxies, stellar clusters, and galaxy clusters are a few examples of real N-body systems one can meet in the context of astrophysics. Of course a huge spectrum of N-body systems appears in every other field of physics. It is desirable to understand the dynamics of the motion of bodies in such systems, a piece of information that is critical to our understanding of the system itself. Especially in the context of astrophysics, real experiments that involve N-body systems are unfortunately unrealistic (galaxies are too big to fit in the lab!). One alternative in our effort toward understanding is numerical experiments using digital computers. Computational physics is without question a new paradigm in science, a new way to get answers, wherever analytics or experiments meet problems too difficult to solve.

Although one understands the interparticle dynamical law, and may have some information about the mass density of an N-body system, it is usually too expensive (in time and resources) to simulate the N-body systems as realistically as needed. Several codes have been developed that can perform N-body simulations. However serious resources of computer time and hardware are necessary in most cases.

Fortunately there may be an alternative, or at least this is what is claimed. The idea is rather simple in first view, although in the physics terrain there are usually subtle dynamical implications associated with any simplification. Every system of N bodies that interacts via a gravitational force (long-range force) generates a bulk potential that characterizes the system as a whole. The idea is

easy to understand if we think that the system of N bodies is characterized by a number density. This number density can be smoothed out to a continuous density. Then using Poisson's equation one is an integration away from analytically defining the potential (although the integral cannot always be solved, one can still find the value of the potential numerically for every point of interest).

Let's translate the previous paragraph into mathematics. To make things simple (but without losing generality) let's assume that the total mass of the system is $M = 1$ and that this system consists of N point masses each of equal mass m. Therefore $m = M/N = 1/N$. The density of this system is discrete (or singular) and can be represented as a sum of N delta functions, each of which represents one singularity (that is one particle). Therefore:

$$\rho(\mathbf{r}) = \frac{M}{N} \sum_{i=1}^{N} \delta(\mathbf{r} - \mathbf{r}_i) \tag{1.1}$$

Now this mass density will generate a potential the form of which can be found via the well-known Poisson's equation:

$$\nabla^2 \Phi = 4\pi G \rho \tag{1.2}$$

where G is the gravitational constant.

The potential generated by the mass density ρ is the following:

$$\Phi_N(\mathbf{r}) = -\frac{GM}{N} \sum_{i=1}^{N} \frac{1}{|\mathbf{r} - \mathbf{r}_i|} \tag{1.3}$$

There is no approximation until this point except that all the particles have the same mass m. The equations are exact and cumbersome. If somebody decides to use these equations to study the evolution of the system he is doomed to use one of the computationally expensive N-body codes.

However all these masses will generate a potential that will characterize the space. If one can express this potential through an analytical formula then one has

a dynamical model that, in principle, closely (how closely will be discussed soon) describes the system of N bodies. If the potential cannot be expressed analytically, still one can express the density analytically, and then compute numerically (via Poisson's equation) the potential for any possible value.

This is a method for simulating a real system, but it has the complication that the N-body potential cannot always be translated into an analytical smooth potential. However, we can follow a different way: There are many cases (common practice in science) in which people use so-called toy models, (models that are described analytically through a simple potential formula and that are believed to be generic). Both of these properties are critical. Simulations of motion in simple analytical potentials are fast and easy to perform. Generic potentials are necessary because one tries to understand the physics characterizing more realistic systems by studying the toy model. If the toy model is not generic one should not expect its results to apply in general to realistic systems. Nongeneric toy models are mathematical ingenuities that have no application to nature (although sometimes applications are discovered years later.)

Now an interesting point: Let's assume one has chosen an analytic potential and has computed its (analytic) density via Poisson's equation. He is now in a position to transform his model to an N-body system. He is thus in a position to play the game exactly the opposite way: from his analytic model to go to an N-body system. This can be done easily by using a numerical program that samples the analytic density. What he produces this way is nothing but a representation of the analytical model by a system of N bodies. In this thesis I deal only with time-independent systems. Thus the N-body analogue of an analytic potential will always consist of bodies that do not move (they have zero velocity). It is reasonable then to "baptize" such a system a "frozen-N" system. So the ultimate

question is: *what is the difference between the dynamics associated with the analytic potential and the dynamics associated with its frozen-N analogue?*

Before I analyze the question even more, please note an important point. It is obvious that the larger N is, the better the analytic potential is represented by its frozen-N analogue. As N increases, the masses become smaller and the typical interparticle distance also becomes smaller. Thus someone might visualize that for $N \to \infty$ the frozen-N potential will exactly coincide with its analytical analogue. The frozen-N environment will be so dense that it will enter the continuous regime, which is the smooth analytical density. This smooth analytical density is exactly what one calls "the continuum limit."

It is important here to understand the main difference between a smooth potential and its frozen-N analogue. An N-body environment is always characterized by discreteness effects. The environment is "grainy," far from the smoothness of the analytical potential. A body moving in the frozen-N environment will feel a bulk smooth potential generated because gravitation is a long-range force. It will also feel "kicks" because of close encounters with the N-body frozen particles. Eventually someone may think of the whole motion as a stochastic process generated by some differential equation, where external potential and a random force play their different roles, and collectively determine the dynamical evolution. (We actually tried that!)

So the main question is how the dynamics in a smooth potential and in its frozen-N analogue compare. Before I analyze this question further it is imperative to describe the existing information relative to this question.

First a numerical result: It has been known since at least 1964 that motion in an N-body system is chaotic [1]. It is very important here (and it will become quite clear later why) to emphasize that by chaotic I mean sensitive dependence on initial conditions (the classical definition of chaos). It is chaos in this sense

that can be quantified by so-called Lyapunov exponents. Later in the introduction I talk more about these exponents. For now notice that an N-body system is always chaotic, even when the smooth analogue is an integrable potential! However after a little thought, this is quite reasonable. An integrable potential possesses symmetries (as many as the degrees of freedom). The phase space has $2n$ dimensions where n is the degrees of freedom. Because of the presence of the discreteness effects, the frozen-N analogue does not possess the same symmetries. Its phase space is more complicated and it has nN dimensions. As a result, an orbit that is regular in the smooth potential can (and in general will) be chaotic in the frozen-N environment.

One might intuitively expect that as N increases, the phase space of a frozen-N system will resemble more the phase space associated with the smooth potential. This means that if an orbit is regular in the smooth potential, then for very large N, in its frozen-N analogue it should be regular or at least approach regularity (always in the sense of sensitive dependence on initial conditions!). The truth however (and the big surprise) is that this does *not* happen. The orbit remains chaotic even for very large N! There is a theoretical explanation of this fact and I will talk more carefully about this in the conclusions. However the claim is that if one perturbs an orbit in an N-body environment, the time scale τ on which the separation of the perturbed from the unperturbed orbit tends to grow will not diverge (will not increase without bound) for $N \to \infty$. There is some disagreement though as to whether τ should converge toward an N-independent value [2] or whether τ should instead slowly decrease with increasing N [3].

Let's go back to numerics. A major motivation for this research was the fact that most of what was done before in the context of chaos in N-body environments focused either on small N and long times of integration, or large N but short times of integration. Little or no work had been done with large N and long times of

integration, a condition needed in order to estimate honest Lyapunov exponents, and therefore to quantify chaos adequately.

A second major point of motivation emerged because of the common use of the a so-called softening parameter (usually denoted as ϵ) in the N-body simulations. First I have to refer to the technical considerations that make the use of the softening parameter attractive if not necessary. If one looks carefully at Formula 1.3 it is obvious that if two particles happen to come very close, the denominator will become very large causing an overflow error [4]. Therefore it is considered a proactive behaviour to slightly manipulate the N-body potential by including in the denominator a small number so to avoid this error:

$$\Phi_N(\mathbf{r}) = -\frac{GM}{N}\sum_{i=1}^{N}\frac{1}{\sqrt{(\mathbf{r}-\mathbf{r}_i)^2+\epsilon^2}} \tag{1.4}$$

However this is not the only reason the softening parameter is included. Larger values of ϵ simply transform the particle into a superparticle, a group that is of many particles [5]. If two of these superparticles happen to come very close the softening parameter will simply put a lower bound in the force of their interaction, which is actually what should happen realistically in an environment of N superparticles.

The value of this idea is of course that one can hope to simulate a realistic system of many bodies using a much smaller number N in the numerical simulation. This is quite a useful idea *but* there is some consequence. Exactly because the softening parameter introduces a lower bound in the interaction force it practically "kills" all the effects of close encounters that are responsible for destabilization of the orbit [6]. This means that it removes all the chaotic effects that ought to be present! Therefore it is not a hyperbole if someone views all simulations done with very large ϵ with a critical eye and a sceptical mind. One last thing to mention about the softening parameter is that its necessity (to avoid overflow errors) makes

it also necessary to add one more element in the definition of the "continuum limit." *The continuum limit is approached when* $\epsilon \to 0$ *and* $N \to \infty$.

Having described what is already known, the next step is to define carefully what answers one is interested in and what questions he has to ask in order to find these answers.

The main question is rather obvious: How close must a system of N bodies be to the continuum limit (i.e. how large must N be) in order for the dynamics of the smooth potential and its analogue frozen-N system to be indistinguishable? The same question can be asked in different terms: For what time scales, i.e. for how long the dynamics be the same? This is an interesting question but very general. The term "dynamics" is of course very broad and involves many measures. The simplest comparison here would be in the context of the motion of single orbits, that is pointwise. In this thesis I examined very carefully this question and I will discuse it extensively. In order to make it clearer: how will two orbits, starting from the same initial condition, evolve in the two different systems, the smooth and the frozen-N? How do they diverge in time and how does this divergence depend on N? How does the divergence law differ for integrable and nonintegrable potentials? We investigated carefully and gave answers to all these questions.

Now the next obvious question involves the quantification of chaos. There are two measures that have been extensively used for this purpose. The first has been already been mentioned: Lyapunov exponents [7, 8]. The mathematical definition of this measure is rather old and for completeness and historical reasons I will include its formal definition:

$$\chi = \lim_{t\to\infty} \lim_{dz\to 0} (\frac{1}{t}) \ln(\frac{\delta z(t)}{\delta z(0)}) \tag{1.5}$$

Of course numerically this measure can never be computed because of the limits (one cannot integrate to infinity). Instead what was computed was the largest

short-time Lyapunov exponents, using a method introduced in 1980 by Bennetin, Galgani et.al. [9] which has since become classic. This method simply involves evolving an orbit and a second slightly perturbed orbit for a short-time (about one dynamical time), then renormalizing the perturbed orbit (to bring the two orbits close again), and then repeating the same until the average Lyapunov exponent converges to an almost constant value.

The second measure which proved to be extremely useful in this series of experiments was the power spectrum of the orbits [7, 8]. It is well known that the power spectrum of a regular orbit is characterized by a few almost discrete frequencies (theoretically they are discrete but this can never be the case for numerical experiments, unless one integrates for $t \to \infty$, a numerical impossibility of course). On the other hand chaotic orbits are characterized by a much more complicated spectrum, that may include a few 'main' frequencies, but also includes lots of other frequencies with smaller but collectively significant power. These extra frequencies give some "grassy" look to the spectrum.

There are still two questions of importance. The first involves the concept of "chaotic mixing" (i.e. the exponential divergence of initially localised chaotic orbits) [10, 11, 12, 13, 14]. How does chaotic mixing take place in an N-body environment? How does it depend on N? And what are the answers to the same questions for regular orbits? An extensive investigation of these issues was also undertaken.

The last question is one of major practical and potentially theoretical interest. Is it possible to simulate motion in a frozen-N environment using a Langevin equation [15, 16]? This means that one has to include in the canonical equations of motion some term that represents a Gaussian process with a white noise power spectrum in order to simulate the random kicks a test particle "feels" as it moves in the frozen-N environment. Could such an approach give results similar to the

results of real N-body simulations? A number of experiments were also performed here with extremely interesting results.

CHAPTER 2
MATHEMATICAL FORMULAS

Hitherto I have refered to what information already exists in work that has been done by other researchers. I have also defined carefully what the questions are and I have given a broad outline about how to get these answers, what experimental procedures, measures, and criteria are necessary. Next I will get more specific about the experimental processes used for this thesis.

Firstly it is necessary to give in detail all the mathematical formulas that describe the smooth potentials which were chosen to be used as well as brief information pertaining to the reasons those potentials were chosen.

In this investigation four smooth potentials were used for the experiments. They are the following:

2.1 Plummer Potential

This is a potential as old as well-known. It was first used in 1911 by H. C. Plummer to fit observations of globular clusters [5]. This potential is integrable. Therefore all orbits are regular. Mathematically it is expressed as:

$$\Phi_P(r) = -\frac{GM}{\sqrt{r^2 + b^2}}. \tag{2.1}$$

This potential can be generated via Poisson's equation by the following density function:

$$\rho_P(r) = \left(\frac{3M}{4\pi b^3}\right)\left(1 + \frac{r^2}{b^2}\right)^{-\frac{5}{2}}. \tag{2.2}$$

with G the gravitational constant, M the mass of the system and b a core radius parameter. For the experiments performed units were chosen so that: $G = M = b = 1$.

2.2 Three-dimensional harmonic oscillator

This is also an integrable potential, and it is extremely simple and computationally fast. Its mathematical formula is:

$$\Phi_E(\mathbf{r}) = \Phi_0 + \frac{1}{2}\left(\omega_a^2 x^2 + \omega_b^2 y^2 + \omega_c^2 z^2\right) \tag{2.3}$$

where ω_a, ω_b, and ω_c are the frequencies in the three different directions and Φ_0 is constant. The values chosen for the experiments performed were: $\Phi_0 \approx -1.00608$, $\omega_a \approx 0.4663$, $\omega_b \approx 0.5508$, and $\omega_c \approx 0.6753$.

The mass density associated with this potential is:

$$\rho_E(\mathbf{r}) = \frac{3M}{4\pi abc} \times m^2 \tag{2.4}$$

with

$$m^2 = \left(\frac{x^2}{a^2} + \frac{y^2}{b^2} + \frac{z^2}{c^2}\right). \tag{2.5}$$

with frequencies ω_a, ω_b, ω_c, related to the axes values a, b, c, in terms of incomplete elliptic integrals [30]. The values we chose for of a, b, and c, were $a = 1.95$, $b = 1.50$, and $c = 1.05$.

2.3 Three-dimensional harmonic oscillator plus a perturbation factor

The perturbation factor simulates a black hole at the center of the system. Because of the perturbation this potential is nonintegrable and admits large regions of global stochasticity. It has been found that the vast majority of orbits (restricted

energetically to $m \leq 1$) in this potential are chaotic [31]:

$$\Phi_{BH} = \Phi_E - \frac{GM_{BH}}{\sqrt{r^2 + \epsilon^2}}, \tag{2.6}$$

with M_{BH} the mass of the black hole and ϵ a softening parameter introduced to avoid overflow errors. G represents as usual the gravitational constant and for the choice of the units used its value is $G = 1$. The choices for the perturbation parameters were: $\epsilon = 10^{-3}$, and $M_{BH} = 10^{-1.5}M \approx 0.0316228M$. The parameters associated with the integrable part were the same as in the previous potential.

The mass density associated with this potential is:

$$\rho_E(\mathbf{r}) = \rho_E + \frac{GM_{BH}}{4\pi}\left(\frac{-3r^2}{(r^2+\epsilon^2)^{\frac{5}{2}}} + \frac{1}{(r^2+\epsilon^2)^{\frac{3}{2}}}\right) \tag{2.7}$$

2.4 A triaxial generalisation of Dehnen potential

This potential does not have an analytic form, but its values can be computed numerically via Poisson's equation. The density associated with this potential is [32]:

$$\rho_D(\mathbf{r}) = \frac{M(3-\gamma)}{4\pi abc} m^{-\gamma}\,(1+m)^{-(4-\gamma)}, \tag{2.8}$$

with

$$m^2 = \left(\frac{x^2}{a^2} + \frac{y^2}{b^2} + \frac{z^2}{c^2}\right). \tag{2.9}$$

where γ and a, b, and c are free parameters. The values chosen for the experiments were: $\gamma = 1$, $a = 1.0$, $b = \sqrt{5.0/8.0}$, and $c = 0.5$. These values have been used to simulate a triaxial galaxy with a central cusp [33]. It has been found numerically that for these values this potential admits a coexistence of large measure of both regular and chaotic orbits[33, 34].

For completeness I will give again here the mathematical formulas associated with the potential and the mass density of frozen-N systems generated by sampling

the mass densities of smooth potentials. The potential is:

$$\Phi_N(\mathbf{r}) = -\frac{GM}{N}\sum_{i=1}^{N}\frac{1}{\sqrt{(\mathbf{r}-\mathbf{r}_i)^2+\epsilon^2}} \tag{2.10}$$

(where I have included the softenting parameter) and it is generated by the density of N discrete masses:

$$\rho(\mathbf{r}) = \frac{M}{N}\sum_{i=1}^{N}\delta(\mathbf{r}-\mathbf{r}_i) \tag{2.11}$$

The main experiment performed was quite straightforward: Integrate some initial condition(s) (test particles) in a smooth potential. Generate frozen-N distributions that correspond to this potential. Then integrate the same initial condition(s) in the frozen-N environment. For every intergation (smooth or frozen-N) two kinds of data were recorded: (a) the orbital data, and (b) the largest short-time Lyapunov exponents associated with the orbits of the test particles.

The integrations for the smooth potentials were performed by an adaptive time step Runge-Kutta algorithm [40]. In the case of the Dehnen potential a code written by C. Siopis for his Ph.D dissertation was used [35]. The integrations in the frozen-N environments were realised by a direct summation code written by the author. All integrations conserved energy to at least one part in 10^{-4}. The routine that computed the Lyapunov exponents was based on a well known algorithm by Benettin, Galgani et.al [9]. The sampling of the density distributions was realized for the Plummer potential by a von Neumann rejection method, and for the rest of the cases by a code written by the author that was based on a new algorithm.

CHAPTER 3
INTEGRABLE POTENTIALS

Since the mathematical formulation of the numerical experiments has been set up we are ready to proceed to the description of the experiments. In this chapter I will talk exclusively about the experiments and results related to integrable potentials. In the next chapter I will proceed to the nonintegrable potentials.

3.1 Divergence Laws

The first series of experiments were performed using the Plummer potential. The purpose was to identify first the dynamical behaviour in a generic integrable system, without the complications introduced by the chaotic behaviour of nonintegrable potentials. The second step was to perform the same experiments in the also integrable (but nongeneric) three-dimensional harmonic oscillator and see if similar behaviour was observed. Then having a clear picture about what happens in the integrable case we could proceed to the more complicated nonintegrable case.

All integrations were performed for evolution times that physically correspond to about 100 dynamical times. Such long times were both necessary and important for the fair treatment of the problem because: (a) $100t_D$ (for galaxies) is a time scale equivalent to the age of the universe, so it is the natural time scale for the evolution we wanted to simulate, and (b) (a more technical consideration) integration times of such length are required numerically since they are necessary for the Lyapunov exponents to converge.

The obvious first comparison was between the evolution of initial conditions $(\mathbf{r}_0, \mathbf{v}_0)$ integrated in the smooth potential and in the corresponding frozen-N environment. This comparison should be performed for different N and for variable

values of the softening parameter. This way a clear first picture would emerge about the validity of the continuum limit. Twenty different frozen-N distributions were generated for each choice of N. The number of particles for the frozen-N environments varied from $N = 10^{2.5}$ to $N = 10^{5.5}$. The softening parameter also varied from $\epsilon = 10^{-1}$ to $\epsilon = 10^{-5}$. The closer to zero ϵ is, the more "honest" the frozen-N simulation is considered.

Intuitively one would expect that for sufficiently short times the two orbits will coincide, but that for longer times they should diverge because the smooth and the frozen-N potential are only approximately similar. The differences the body experiences during his motion in the two environments should eventually translate into a divergence of the two orbits.

Therefore two meaningful questions can easily arise: (a) How do the position and velocity divergence between the smooth characteristic and the frozen-N orbit evolve in time? Do they evolve as a power law or exponentially? (b) How does the growth time of this divergence depend on the number of particles N? The answer to these questions is quite critical for the validity of the continuum limit at a pointwise level. Equally important, however, is to ask the same two questions about the angular momentum, which is an invariant of motion for the Plummer potential since it is a spherically symmetric system.

First let's consider these questions at the most elementary level and examine a crude comparison between two orbits, starting from the same initial condition, but with the first evolved in the smooth potential and the second in the frozen-N environment.

It is probable that the first naive expectation (or guess!) someone would have about the law that governs the divergence of the two orbits in the two different regimes would be that it is exponential, since it is known that the frozen-N orbits are chaotic. However exponential divergence was definitely not observed. Rather

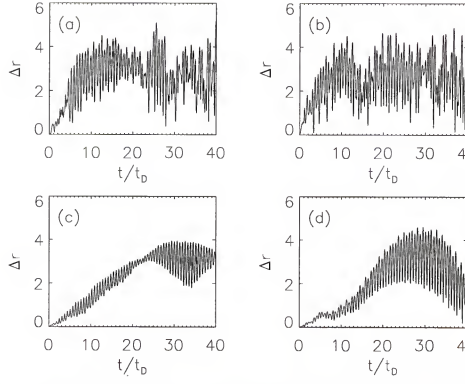

Figure 3.1: (a) The deviation $\Delta r = |\mathbf{r} - \mathbf{r}_s|$ from the smooth potential characteristic for one representative frozen-N orbit evolved with $\epsilon = 10^{-4}$ and $N = 10^3$. (b) Another frozen-N orbit evolved with the same ϵ and N for the same initial condition. (c) and (d) the same for $N = 10^5$.

what was observed was a power law in time, a striking result! This was true not only for small values of ϵ, where frozen-N orbits are very chaotic, but also for larger values of ϵ, where orbits tend to be more regular because of the suppression of chaos. Figure 3.1 exhibits the quantity $\Delta r = |\mathbf{r} - \mathbf{r_s}|$ for a typical orbit evolved in the frozen-N environment with $\epsilon = 10^{-4}$. The first two panels are for $N = 10^3$, and the latter two for $N = 10^5$. It is evident that, rather than exponential, the growth of Δr is roughly linear in time.

This divergence continues until the typical separation has become comparable to the size of the configuration space region to which the orbits are confined, and the frozen-N orbit has become completely decorrelated in appearance from the smooth potential characteristic. This means that the frozen-N orbits do not stay close to the smooth characteristic, which would be the case if the divergence was terminated at comparatively small separations.

Now let's examine the full statistics of the problem using moments that involve all 20 simulations in the frozen-N configurations. Two types of moments were used. First let's denote the positions and velocities of the $n = 20$ different trajectories (for one initial condition) in the 20 different frozen-N environments as $(\mathbf{r}_i(t), \mathbf{v}_i(t))$, $(i = 1, ..., n)$, and the position and velocity of the smooth characteristic (for the same initial condition) as $(\mathbf{r}_s(t), \mathbf{v}_s(t))$. The first type of moment that was used (for the position variables) included the following:

$$\langle \mathbf{r} \rangle = \frac{1}{n} \sum_{i=1}^{n} \mathbf{r}_i \tag{3.1}$$

and

$$Dr^2 = \langle |\mathbf{r}_i - \langle \mathbf{r} \rangle|^2 \rangle \equiv \frac{1}{n} \sum_{i=1}^{n} |\mathbf{r}_i - \langle \mathbf{r} \rangle|^2 \tag{3.2}$$

The second type included:

$$\Delta r^2 \equiv \langle |\mathbf{r} - \mathbf{r}_s|^2 \rangle = \frac{1}{n} \sum_{i=1}^{n} |\mathbf{r}_i - \mathbf{r}_s|^2 \tag{3.3}$$

and

$$\delta r^2 = \langle |\langle \mathbf{r} \rangle - \mathbf{r}_s|^2 \rangle \tag{3.4}$$

The same quantities were also generated for the velocity $\mathbf{v}$ and for the angular momentum $\mathbf{J} = \mathbf{r} \times \mathbf{v}$. It was found that the quantities Dr, Δr, and δr exhibit comparatively similar evolutions. For this reason only Δr will be discussed.

Before I proceed, I will refer very briefly to an analytical consideration. Let's denote by R_s^2 the mean value of r^2 associated with the smooth characteristic. Now given that the frozen-N orbits conserve energy, the average distance from the origin should be the same as for the smooth characteristic, (that is R_s^2) so that:

$$\langle r^2(t) \rangle \to R_s^2 \quad \text{for} \quad t \to \infty \tag{3.5}$$

Also one expects that:

$$\langle \mathbf{r}(t) \cdot \mathbf{r_s}(t) \rangle \to 0 \quad \text{for} \quad t \to \infty \tag{3.6}$$

so that it may be infered that $\Delta \mathbf{r}^2 \to 2R_s^2$.

It follows that one can use $2R_s^2$ as a normalization factor and plot the quantity $\Delta r / \sqrt{2R_s^2}$ instead of Δr. The normalized quantity then should saturate towards unity, reflecting the fact that the orbits have become completely different from each other.

This is what can actually be seen in Figure 3.2. The left-hand two panels show the evolution for integrations with $\epsilon = 10^{-4}$ for $N = 10^3$ and $N = 10^5$. The right-hand panels exhibit the same data but now subjected to a boxcar averaging.

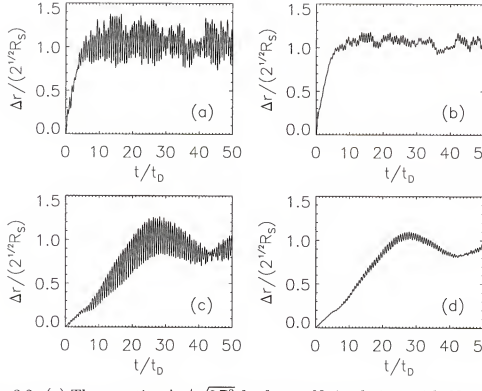

Figure 3.2: (a) The quantity $\Delta r/\sqrt{2R_s^2}$ for frozen-N simulations with $N = 10^3$ and $\epsilon = 10^{-4}$. (b) The same data subjected to boxcar averaging over an interval $t = t_D$. (c) and (d) The same for $N = 10^5$.

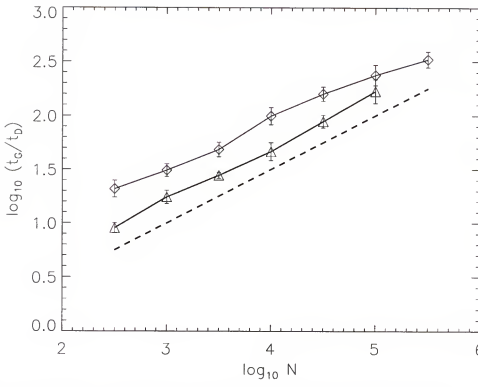

Figure 3.3: Best fit values of the time scale $t_G(N)$ associated with the divergence of smooth and frozen-N orbits for two different initial conditions: $\Delta r/R_s = \Delta v/V_s \equiv t/t_G$. The dashed line has slope 1/2, corresponding to an $N^{1/2}$ dependence.

Let's discuss about what happens on these plots. I have already explained why the saturation should happen at a value of unity. The large envelopes associated with the curves in the left-hand panels reflect the fact that at late times the frozen-N orbits oscillate about the value of unity. Now two additional facts are quite obvious from this graph. The first is that the evolution in time is linear. And the second is that the growth time of the divergence (i.e. the slope of the curve from time zero to the saturation time) depends on the number N of the frozen particles. It is obvious that the divergence grows more slowly as N increases, which is what someone would intuitively expect, since larger N means that the frozen-N potential resembles the smooth potential more closely. Figure 3.3 exhibits $\log_{10}(t_G/t_D)$ as a function of $\log_{10} N$ for two different initial conditions integrated for $\epsilon = 10^{-5}$.

Thus the mathematical formula that expresses the observed behaviour can be written as:

$$\frac{\Delta r}{r_s} = \frac{t}{t_G}. \tag{3.7}$$

Here t_G represents the growth time and is given by:

$$t_G \approx A_G N^p t_D \tag{3.8}$$

where A is of order unity and $p \approx 0.5$. The complete law is thus:

$$\frac{\Delta r}{r_s} \propto \frac{1}{\sqrt{N}} \frac{t}{t_D} \tag{3.9}$$

The same law applies for Δv:

$$\frac{\Delta v}{v_s} \propto \frac{1}{\sqrt{N}} \frac{t}{t_D} \tag{3.10}$$

The square root dependence on N of both Δr and Δv might suggest diffusion but the time dependence is definitely not square root. However such a dependence in time was observed for the corresponding statistical quantities associated with angular momentum. There (for small ϵ) results suggest the following dependence:

$$\frac{\Delta J^2}{J_s^2} = \frac{t}{t_J} \tag{3.11}$$

where J_s is the magnitude of the angular momentum associated with the smooth characteristic and

$$t_J \approx A_J N^p t_D \tag{3.12}$$

where $A_J \approx 3A_G$ and $p \approx 0.5$. The dependence of $\log_{10}(t_J/t_D)$ versus $\log_{10} N$ can be seen in Figure 3.4.

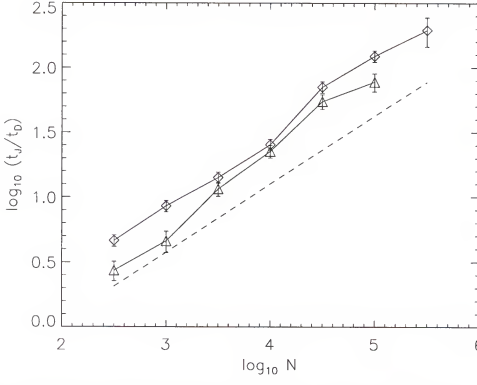

Figure 3.4: Best fit values of the time scale $t_J(N)$ associated with changes in angular momentum for frozen-N orbits for two different initial conditions: $\Delta J^2/J_s^2 \equiv t/t_J$. The dashed line has slope 1/2, corresponding to an $N^{1/2}$ dependence.

3.2 Average Short-time Lyapunov Exponents

Largest short-time Lyapunov exponents have been used extensively as the principal diagnostic of chaos. The aim here was to compute the average short-time Lyapunov exponent characterizing orbits starting from the same initial condition and evolved in the 20 different frozen-N configurations, for different values of N and ϵ. The dependence of the average short-time Lyapunov exponent on N and ϵ can be seen in Figures 3.5 and 3.6. It is obvious from Figure 3.5 that the size of the Lyapunov exponent decreases as ϵ increases. This is an expected behaviour. Since the potential is integrable the observed chaos is generated completely by the close encounters of the test particles with the field particles. By increasing ϵ, a minimum impact parameter is imposed to the system, so that the destabilization of the orbit (associated with the close encounters) that leads to chaotic behaviour, is suppresed.

However when ϵ is sufficiently small, its precise value seems to be immaterial. This happens because as long as ϵ is smaller than the value of the closest separation between the test particle and the field particles during the integration, the test particle feels practically an unsoftened potential. The obvious point derived from these results is that the introduction of large softening definitely suppresses the perturbations that can lead to chaotic behaviour.

When ϵ is large the value of the Lyapunov exponent decreases with increasing N. The reason is obvious: For a system of fixed size, as N increases the typical distance between particles decreases. For very small N this distance is still large, larger than the value of the softening parameter, so that the close encounters that generate chaos are not suppressed. However as N increases, the interparticle distance decreases. When this distance becomes smaller than ϵ, many weak encounters get suppresed, a fact that causes the observed decrease in the value of the Lyapunov exponents.

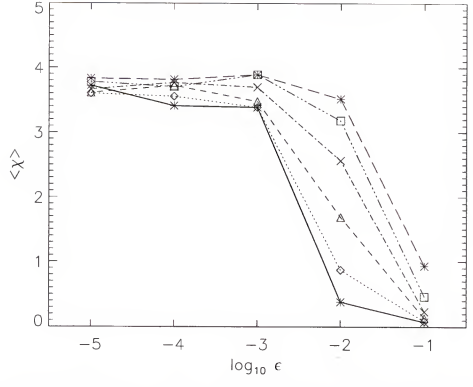

Figure 3.5: Mean short-time Lyapunov exponent $\langle\chi\rangle$ as a function of softening parameter ϵ for $N = 10^5$ (solid line), $N = 10^{4.5}$ (dotted), $N = 10^4$ (dashed), $N = 10^{3.5}$ (dot-dashed), $N = 10^{3.0}$ (triple-dot dashed), and $N = 10^{2.5}$ (broad dashed). The integrations were all performed for a single 'typical' initial condition.

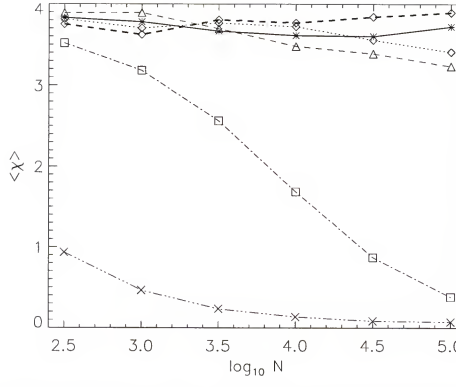

Figure 3.6: Mean short-time Lyapunov exponent $\langle\chi\rangle$ as a function of particle number N for $\epsilon = 10^{-5}$ (solid line), $\epsilon = 10^{-4}$ (dotted), $\epsilon = 10^{-3}$ (thin-dashed), $\epsilon = 10^{-2}$ (dot-dashed), and $\epsilon = 10^{-1}$ (triple-dot dashed), all computed for the initial condition used to generate Figure 3.5. The short-time $\langle\chi\rangle$ for a different initial condition corresponding to a smooth radial orbit, again evolved with $\epsilon = 10^{-5}$, is indicated by the curve with thick dashes.

However when ϵ is very small the Lyapunov exponents seem almost independent of N. It is possible to understand qualitatively the physical reason for this. Integrable potentials do not exhibit chaos. This means that all the chaos observed in their frozen-N analogues must be associated with discreteness effects that perturb the orbits because of close encounters. This suggests that the time scale for the growth of a small initial perturbation can be calculated if we consider the tidal effects associated with two particles separated by some typical interparticle distance. The tidal acceleration is:

$$\delta\ddot{\mathbf{r}} = (\delta\mathbf{r} \cdot \nabla)\mathbf{a} \sim \frac{Gm}{r^3}\delta\mathbf{r} \tag{3.13}$$

where r is the separation and m the particle mass. Suppose however that:

$$r \sim n^{-\frac{1}{3}} \sim N^{-\frac{1}{3}} R_{sys} \tag{3.14}$$

with n the characteristic number density and R_{sys} the size of the system. It then follows dimensionally that the time scale that characterizes the interaction is:

$$t_i \sim \frac{1}{\sqrt{G\rho}} \tag{3.15}$$

which is independent of N and practically comparable to the dynamical time (also independent of N).

3.3 Power Spectra and Complexities

The results described in the previous paragraph about the average short-time Lyapunov exponents suggest clearly that for small ϵ the orbits remain chaotic regardless of the value of N. Let's now have a look at the visual appearance of a typical orbit in the frozen-N configuration for different values of N ($10^{2.5} - 10^{5.5}$) and $\epsilon = 10^{-5}$ (Figure 3.7). The final panel exhibits the behaviour of the orbit in the smooth potential environment. It is very clear from this picture that as N

increases: (a) the orbit looks less chaotic, and (b) it resembles more closely the smooth characteristic.

In order to visualize in a more quantitative fashion this transformation towards smoother orbital behaviour as N increases, one can consider the power spectrum of the orbit. The power spectra that correspond to the orbits in Figure 3.7 can be seen in Figure 3.8. First let's have a look at the power spectrum of the smooth orbit. It is clear that the power is concentrated into two main frequencies that are very sharp (this is expected for a regular orbit). Now for very small N the power spectrum exhibits a variety of different frequencies, something that characterizes a chaotic orbit. However, as N increases the power spectrum changes to resemble more closely the spectrum of the smooth characteristic, with the power concentrated into smaller number of frequencies, and the "grass" of frequencies associated with chaos largely eliminated.

In order to quantify this result more objectively, the next logical step is to compute the complexity of the orbits, i.e. the number of frequencies in the Fourier spectrum that contains an appreciable amount of power [29]. Two measures of complexity were defined. The first $f_{0.1}$ is the sum of the number of frequencies $f_{0.1,x}$, $f_{0.1,y}$, and $f_{0.1,z}$ which have more than 10% as much power as the peak frequencies for ω_x, ω_y, and ω_z:

$$f_{0.1} = f_{0.1,x} + f_{0.1,y} + f_{0.1,z} \tag{3.16}$$

The second measure $k_{0.95}$ is defined correspondingly for the sum of the number of frequencies required to capture 95% of the power in the x,y, and z directions:

$$k_{0.95} = k_{0.95,x} + k_{0.95,y} + k_{0.95,z} \tag{3.17}$$

The graph of both measures versus $log_{10}N$ can be seen in Figure 3.9. With increasing N both these quantities decrease.

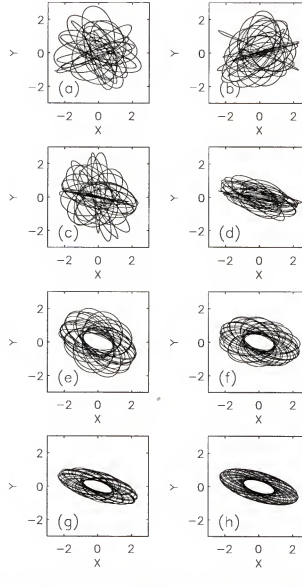

Figure 3.7: The x-y projection of representative frozen-N orbits generated from the same initial condition, evolved for $t = 25t_D$ with $\epsilon = 10^{-5}$. (a) $N = 10^{2.5}$. (b) $N = 10^3$. (c) $N = 10^{3.5}$. (d) $N = 10^4$. (e) $N = 10^{4.5}$. (f) $N = 10^5$. (g) $N = 10^{5.5}$. (h) The x-y projection of the same initial condition evolved in the smooth potential.

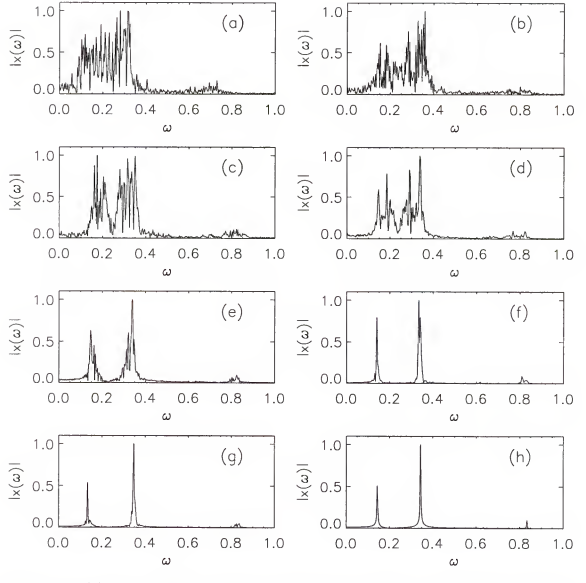

Figure 3.8: (a) The Fourier transformed $|x(\omega)|$ for one frozen-N integration of the initial condition used to generate Figure 3.7, evolved with $\epsilon = 10^{-5}$ and $N = 10^{2.5}$. (b) The same for $N = 10^3$. (c) $N = 10^{3.5}$. (d) $N = 10^4$. (e) $N = 10^{4.5}$. (f) $N = 10^5$. (g) $N = 10^{5.5}$. (h) $|x(\omega)|$ for a characteristic in the smooth potential with the same initial condition, with data recorded at the same intervals for the same total integration time.

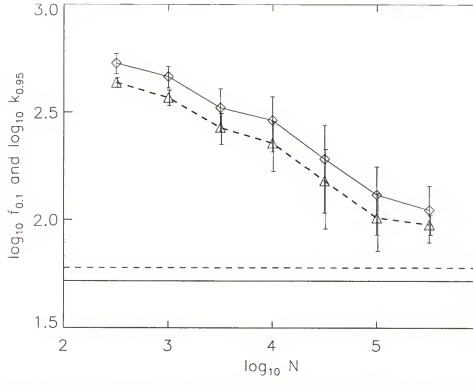

Figure 3.9: Two probes of the complexity of frozen-N orbits for an ensemble of orbits with the same initial condition evolved with $\epsilon = 10^{-5}$. The solid curve exhibits $f_{0.1}$, the number of frequencies which have power equal to at least 10% of the power in the peak frequencies. The dashed curve exhibits $k_{0.95}$, the number of frequencies required to capture 95% of the total power. The vertical lines show $f_{0.1}$ and $k_{0.95}$ for a smooth characteristic generated identically from the same initial condition, thus exhibiting the intrinsic limitations associated with the discrete time series of data points.

CHAPTER 4
NONINTEGRABLE POTENTIALS

4.1 Divergence Laws

In order to investigate the law characterizing the divergence of a chaotic orbit moving in a smooth nonintegrable potential from an orbit starting from the same initial condition but evolving in the frozen-N analogue of the smooth potential, the three-dimensional harmonic oscillator plus perturbation potential (Equation 2.6) was used.

Here the same statistical moments were used as for the integrable potential case. The definitions can be seen in the Chapter 3 (Equations 3.1-3.4) and there is no need to repeat them here. A number of simulations were performed for a statistical sample of 800 test particles starting from initial conditions that in the smooth potentials evolved as "wildly" chaotic orbits (the typical Lyapunov exponent was $\chi = 0.055$). The results of these simulations are exhibited in Figure 4.1. It is obvious that the position divergence evolves linearly in time, the same way that it evolved for the integrable case. The same is true for the velocity divergence.

However there is an important difference between the integrable and nonintegrable cases. The growth time of the divergence was found in the integrable case to depend on the square root of N. In the nonintegrable case this is no longer true. Now the dependence is the following:

$$t_G \approx A_G(\ln N)t_D \tag{4.1}$$

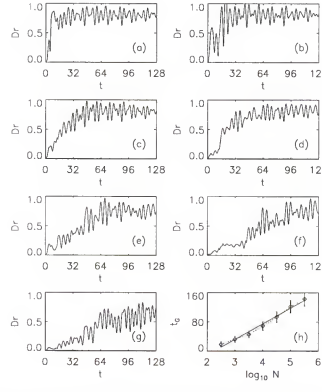

Figure 4.1: The mean separation, Dr, between frozen-N orbits and smooth characteristics with the same initial conditions, computed for ensembles of 800 chaotic initial conditions evolved in the potential (2.6) for variable N. (a) $N = 10^{2.5}$. (b) $N = 10^3$. (c) $N = 10^{3.5}$. (d) $N = 10^4$. (e) $N = 10^{4.5}$. (f) $N = 10^5$. (g) $N = 10^{5.5}$. (h) The growth rate $t_G(N)$ extracted from the preceding panels, assuming a linear growth law. The solid line overlays a least squares fit $t_G = A + B \log_{10} N$.

where A_G is of order of unity. So the complete divergence law for the case of nonintegrable potentials can be expressed as:

$$\frac{\Delta r}{r_s} \propto \frac{1}{\ln N} \frac{t}{t_D} \tag{4.2}$$

and for the velocity:

$$\frac{\Delta v}{v_s} \propto \frac{1}{\ln N} \frac{t}{t_D} \tag{4.3}$$

where $(\mathbf{r}_s(t), \mathbf{v}_s(t))$ express the position and velocity of the smooth characteristic.

The last panel of Figure 4.1 shows the logarithmic dependence of the growth time t_G on N.

4.2 Average Short-time Lyapunov Exponents

Average short-time Lyapunov exponents were computed for orbits evolved in the frozen-N environments associated with the nonintegrable three-dimensional harmonic oscillator plus a perturbation potential. The black hole mass was $M_{BH} = 10^{-1.5}$, i.e. substantially smaller than unity. Initial conditions for both wildly chaotic (orbits that explore all of the phase space energetically available to them) and "sticky" chaotic orbits (orbits that remain for some time in a small region of the phase space but eventually escape to explore all the available phase space energetically available to them) were integrated. Also initial conditions that correspond to regular orbits in the smooth potential regime were integrated in frozen-N environments associated with the three-dimensional harmonic oscillator without the black hole, a completely integrable potential. The average Lyapunov exponents for four different initial conditions for every choice of N can be seen in Figure 4.2. Several very important points can be derived from this picture. (a) The sizes of the Lyapunov exponents for the integrable and nonintegrable case are comparable. This means that someone knowing only the size of the Lyapunov exponent of an orbit that has been evolved in a frozen-N environment cannot

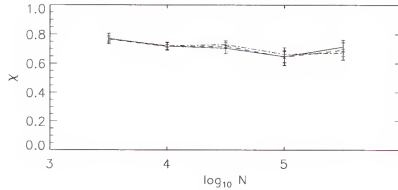

Figure 4.2: Estimates of the largest Lyapunov exponent for orbits evolved in frozen-N realisations of a homogeneous ellipsoid: integrable initial conditions evolved with $M_{BH} = 0$ (solid line), 'sticky' initial conditions evolved with $M_{BH} = 10^{-1.5}$ (dashed line), and 'wildly chaotic' initial conditions with $M_{BH} = 10^{-1.5}$ (dot-dashed line).

know if this orbit will evolve regularly or chaotically in the smooth potential environment. (b) For different numbers of particles N the size of the Lyapunov exponents for nonintegrable potentials is again nearby constant. Recall that the same is true for integrable potentials (both the three-dimensional harmonic oscillator and the Plummer potential in the last chapter exhibited the same behaviour). (c) The typical values of the Lyapunov exponents of orbits evolved in the frozen-N configurations (~ 0.8) are very large compared to the values associated with typical chaotic orbits evolved in the smooth potential (~ 0.055 for wildly chaotic orbits and ~ 0.022 for "sticky" chaotic orbits).

The last point is very important. The Lyapunov exponents that characterize the chaotic orbits in smooth environments are associated with the effect the bulk potential has on the orbit. Therefore they probe a macroscopic effect. On the other hand the large Lyapunov exponents that characterize the orbits in frozen-N environments are associated with the discreteness effects, that is, a microscopic effect. The chaotic effect associated with the bulk potential is still present in the frozen-N configuration but it is so small that it is practically "washed out" by the microscopic chaos generated by the discreteness effects.

4.3 Power Spectra and Complexities

The same effects that were observed for the power spectra and visual appearance for the integrable potentials, were also observed for the nonintegrable potentials. A chaotic orbit evolved in a smooth potential is characterized by a very complex power spectrum. Therefore the motion is characterized by many frequencies (the complexity is large). The same orbit evolved in the frozen-N analogue of the nonintegrable smooth potential will have an even more complex power spectrum if N is small but as N increases and the continuum limit is approached this power spectrum will resemble closer the spectrum of the orbit evolved in the smooth potential. The same of course happens to the visual appearance of the orbit.

4.4 Transitions Between Regular and Chaotic Behaviour

In a frozen-N environment it is possible for an orbit to "jump" from the regular regime to the chaotic one and vise versa. This happens because discretenss effects can push the orbit from a path that corresponds in the smooth regime to a chaotic orbit, to a new path that corresponds in the smooth regime to a regular orbit, or vice versa. This of course is a behaviour that can be observed only for cases of potentials that admit significant measures of both regular and chaotic orbits. One example of such a potential is the triaxial generalisation of the Dehnen potential described in Chapter 2.

The first hint that such transitions do happen is given by the time evolution of the divergence Dr for two different ensembles of initial conditions, one that evolves regularly and one that evolves chaotically in the smooth regime. The evolution of the divergence can be seen in Figure 4.3. What is clear is that the growth time for both ensembles is comparable especially for small N. For larger N the divergence grows slower for regular orbits as it is expected. The fact that for smaller N the

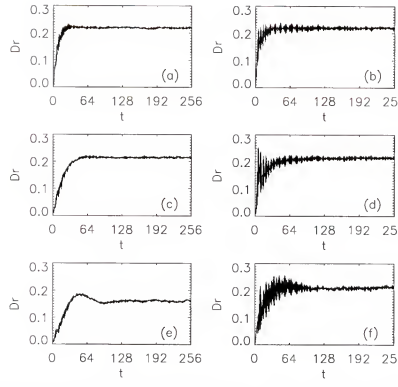

Figure 4.3: The quantity Dr for two different initially localised ensembles of 'sticky' chaotic orbits with the same (low) energies, each evolved in frozen-N realisations of the Dehnen potential. (a) A 'regular' ensemble with $N = 10^4$. (b) A 'chaotic' ensemble with $N = 10^4$. (c) The 'regular' ensemble with $N = 10^{4.5}$. (d) The 'chaotic' ensemble with $N = 10^{4.5}$. (a) The 'regular' ensemble with $N = 10^5$. (b) The 'chaotic' ensemble with $N = 10^5$.

growth times are comparable can be explained as transitions of significant numbers of orbits from regular to chaotic and vice versa.

In order to quantify more carefully these transitions the following experiment was performed. Snapshots of the orbital data of the orbits evolved in frozen-N environments (i.e. the positions and velocities of the particles at times t_0, t_1, t_2 etc.) were used as initial conditions for integration in the corresponding smooth potential. Suppose for example, that an initial condition $(\mathbf{r_0}, \mathbf{v_0})$ corresponding to a chaotic orbit in the smooth regime, is integrated in a frozen-N environment and that at time t (where its coordinates are $(\mathbf{r}, \mathbf{v})$), it has jumped to a regular path. If

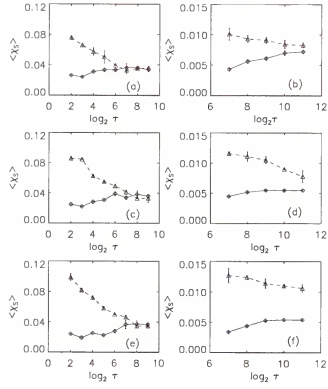

Figure 4.4: The mean Lyapunov exponent $\langle \chi_S \rangle$, for ensembles evolved in the smooth Dehnen potential, selecting as initial conditions the final phase space coordinates of orbits that had been evolved in frozen-N potentials for some time τ. (a) Initially regular (solid line) and chaotic (dashed line) low energy orbits evolved with $N = 10^4$. (b) Initially regular (solid line) and chaotic (dashed line) higher energy orbits evolved with $N = 10^4$. (c) The same as (a) but for $N = 10^{4.5}$. (d) The same as (b) but for $N = 10^{4.5}$. (e) The same as (a) but for $N = 10^5$. (f) The same as (b) but for $N = 10^5$.

someone were to evolve the initial condition $(\mathbf{r}, \mathbf{v})$ in the smooth potential he would compute a Lyapunov exponent that converges to zero.

The results of this experiment are exhibited in Figure 4.4 where the left panels correspond to low energies and the right panels correspond to high energies. It is obvious that the average Lyapunov exponent decreases for the initially chaotic ensembles and increases for the initially regular ensembles. The two lines move towards convergence. This convergence happens faster for smaller N than for larger N, which is a consequence of the stronger discreteness effects associated with small N.

The fact that the regular orbits approach the convergence line faster is a manifestation of the phase space structure of the Dehnen potential. Ensembles of regular orbits correspond to box orbits which pass very close to the center of the system, but close to the center chaotic and regular orbits are entangled in a very complex fashion which makes transitions comparatively easy.

CHAPTER 5
CHAOTIC MIXING

A very interesting question associated with, but not limited to, the question of the validity of the continuum limit is how ensembles of initially localised orbits evolved in a frozen-N environment disperse in the phase space. This question was examined for three different types of ensembles: regular, "sticky" chaotic, and wildly chaotic orbits. It is also very important to compare the behaviour of the dispersion for every type of initial condition with its corresponding dispersion in the smooth potential.

In order to quantify the data the evolution of the dispersion was computed. The dispersion is expressed mathematically as:

$$\sigma_r^2 \equiv \langle r^2 \rangle - \langle r \rangle^2 \tag{5.1}$$

where

$$\langle r^p \rangle = \frac{1}{n} \sum_{i=1}^{n} (x_i^2 + y_i^2 + z_i^2)^{\frac{p}{2}} \tag{5.2}$$

The first potential investigated was the three-dimensional harmonic oscillator (Equation 2.3). Since the smooth potential in this case is integrable and since for this particular potential all orbits oscillate with the same frequency there is no phase mixing of the orbits in the smooth environment. The initial conditions stay as localised as they were in the beginning of the evolution. However in the frozen-N analogue of this potential there is a dispersion of the orbits that grows as

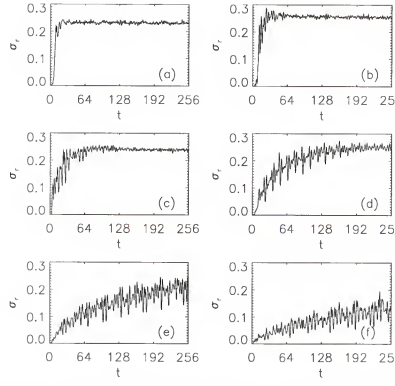

Figure 5.1: The configuration dispersion σ_r associated with an initially localised ensemble evolved in frozen-N realisations of the integrable ellipsoid potential (2.5) for variable N. (a) $N = 10^{2.5}$. (b) $N = 10^3$. (c) $N = 10^{3.5}$. (d) $N = 10^4$. (e) $N = 10^{4.5}$. (f) $N = 10^5$.

a square root of time. The formula that expresses this evolution is given as follows:

$$\sigma_r = (\frac{t}{t_G})^{\frac{1}{2}} \tag{5.3}$$

where t_G is the growth time:

$$t_G = A_G N t_D \tag{5.4}$$

with A_G is of order unity and t_D represents the dynamical time. The evolution of σ_r^2 is exhibited in Figure 5.1 for different values of N.

The evolution of initially localised ensembles of initial conditions was also computed for the case of the Plummer potential (Equation 2.1). This potential is characterized by periodic orbits that oscillate with different frequencies, so that

there is linear phase mixing even in the smooth potential ($\sigma \propto t$). The time evolution of the dispersion was different for different values of N. For small N the dispersion grows as $t^{1/2}$ but for larger N the dependence becomes linear. This is completely understandable. When N is still small discreteness effects are quite strong, so that a diffusion process ($\sim t^{1/2}$) should be expected. As N increases the frozen-N environment approaches the continuum limit and a behaviour similar to that in the smooth potential (which was $\sim t$) should be observed.

The time evolution of dispersion for different N can be seen in Figure 5.2. For $N < 10^4$ the square root law dominates but for larger N the behaviour approaches more and more the evolution that characterizes the smooth potential (last panel) which is linear. The spread of σ_r is reduced for smaller N because the discreteness effects "fuzz out" the systematic oscillations associated with strictly periodic orbits in the unperturbed potential.

The three-dimensional harmonic oscillator plus a perturbation term (Equation 2.6) is a non-integrable potential where almost all the orbits are chaotic. The dispersion in this case evolves roughly exponentially in time and discreteness effects only serve to accelerate this growth.

An example of the growth in dispersion for wildly chaotic orbits the evolution can be seen in Figure 5.3. The evolution of the dispersion σ_r is not strictly exponential but is clearly faster than the exponential growth associated with the smooth potential. This exponential evolution is not the only difference from the case of regular orbits integrated in the Plummer case. Another very important difference is that σ_r for regular orbits integrated with N as small as $10^{4.5}$ resembles the σ_r evolution in the corresponding smooth potential. By contrast it is clear that, for the wildly chaotic orbits this is no longer true. It is obvious that even for N as large as $10^{5.5}$ phase mixing happens much faster than in the corresponding smooth potential.

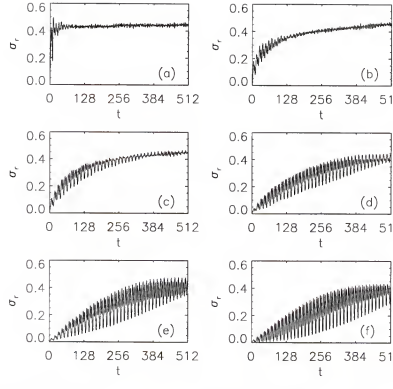

Figure 5.2: The configuration dispersion σ_r associated with an initially localised ensemble evolved in frozen-N realisations of the integrable Plummer potential (2.2) for variable N. (a) $N = 10^3$. (b) $N = 10^{3.5}$. (c) $N = 10^4$. (d) $N = 10^{4.5}$. (e) $N = 10^5$. (f) Evolution in the smooth potential.

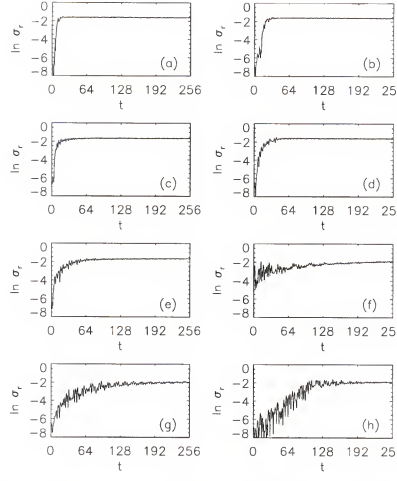

Figure 5.3: The configuration dispersion σ_r associated with an initially localised ensemble of wildly chaotic orbits evolved in frozen-N realisations of the nonintegrable potential (2.6) for variable N. (a) $N = 10^{2.5}$. (b) $N = 10^{3}$. (c) $N = 10^{3.5}$. (d) $N = 10^{4}$. (e) $N = 10^{4.5}$. (f) $N = 10^{5}$. (g) $N = 10^{5.5}$. (h) Evolution in the smooth potential.

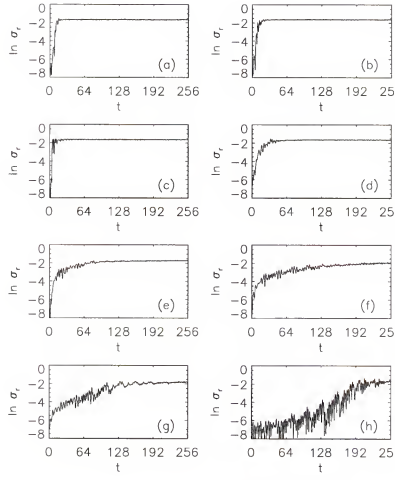

Figure 5.4: The configuration dispersion σ_r associated with an initially localised ensemble of 'sticky' chaotic orbits evolved in frozen-N realisations of the nonintegrable potential (2.6) for variable N. (a) $N = 10^{2.5}$. (b) $N = 10^{3}$. (c) $N = 10^{3.5}$. (d) $N = 10^{4}$. (e) $N = 10^{4.5}$. (f) $N = 10^{5}$. (g) $N = 10^{5.5}$. (h) Evolution in the smooth potential.

Analogous simulations were also performed for ensembles of "sticky" chaotic orbits and the evolution of their dispersions σ_τ for different values of N can be seen in Figure 5.4. For $N \leq 10^4$ discreteness effects are still strong and the "stickiness" is not clearly manifested, but for larger N the growth of σ is slower than for the "sticky" ensemble exhibited in Figure 5.3. It is important to note that the dispersion saturates in a time much longer than the corresponding time required for the wildly chaotic orbits.

CHAPTER 6
LANGEVIN DESCRIPTION

One of the most interesting issues investigated in this thesis was to what extent it is possible to simulate motion in a frozen-N environment using a Langevin description. The Langevin description simply consists of the Hamiltonian equations of motion that are derived for a smooth potential plus two more terms: a term that simulates the dynamical friction generated physically by the drag of the medium, and a term that simulates the random kicks the test particle 'feels' because of the close encounters with the field particles. Therefore the general form of the Langevin equation is:

$$\frac{d^2 r_a}{dt^2} = -\nabla_a \Phi - \eta \frac{dr_a}{dt} + F_a, \qquad a = x, y, z. \tag{6.1}$$

where η can in principle depend on $\mathbf{r}$ and $\mathbf{v}$ but for the experiments performed it had a constant value, and F_a represents a Gaussian white noise. F_a can be completely characterized by its first moment and its correlation function. Its first moment is:

$$\langle F_a(t) \rangle = 0, \qquad (a, b = x, y, z)$$

and

$$\langle F_a(t_1) F_b(t_2) \rangle = 2\eta\Theta\delta_{ab}\delta_D(t_1 - t_2), \tag{6.2}$$

where the "temperature" Θ is associated with internal degrees of freedom of the system. It can be put equal to the initial energy of the initial condition in order to ensure that the average energy of the orbit remains unchanged. It is clear that

the noise depends on the friction and the temperature of the system, which is a result of one of the most important theorems in the statistical mechanics, the Fluctuation-Dissipation theorem. This profound theorem connects the response of a system to its properties.

However since the energy for the frozen-N orbits remains constant, while for the 'noisy' orbits it does not, it was imperative to include in the numerical program an energy conservation routine that corrected slightly the orbit. This routine was renormalising the velocity at each time step by an overall factor, i.e. $\mathbf{v}(t+\delta t) \rightarrow a\mathbf{v}(t+\delta t)$ with a so chosen that $E(t+\delta t) = E(t)$.

At this point there is a hidden technicality associated with the Langevin description of motion in a frozen-N potential. What happens in the frozen-N environments clearly depends on N. The Langevin description depends on the choice of η, which means that there must be a logical way to associate the right η with the right N. The argument we used to connect the two quantities is straightforward. The value of η defines a characteristic relaxation time $t_R = 1/\eta$. This is the time needed in order for significant changes in conserved quantities like energy to be observed (for a self-gravitating system). On the other hand it is well-known that discreteness effects associated with close encounters in an N-body system impose a relaxation time which is: $t_R \propto (\ln N/N) t_D$ where t_D is the characteristic dynamical time. The last two formulas give a clear way to correspond values of η to values of N although it is still crude and needs refinement (I will talk later about this). The obvious formula that connects the two quantities is $\eta \propto \ln N/N$ which for large N becomes $\eta \propto 1/N$.

A good question before I proceed is what is the law governing the divergence between perturbed and unperturbed regular and chaotic orbits moving in a smooth potential and subjected to friction and white noise. The behaviour is quite different for the two kinds of orbits: The divergence of regular orbits is characterized by

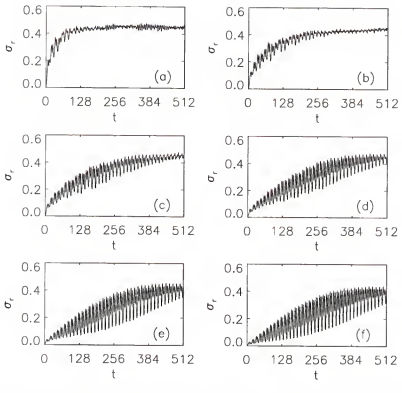

Figure 6.1: The configuration dispersion σ_r associated with an initially localised ensemble evolved in the smooth Plummer potential (2.2), perturbed by noise with $\Theta = 1.0$ and variable η. (a) $\eta = 10^{-3}$. (b) $\eta = 10^{-3.5}$. (c) $\eta = 10^{-4}$. (d) $\eta = 10^{-4.5}$. (e) $\eta = 10^{-5}$. (f) $\eta = 10^{-5.5}$.

a power law. Alternatively, at least for weak perturbations the divergence for chaotic orbits is characterized by an exponential law with a rate that is comparable to the largest short-time Lyapunov exponent of the unperturbed orbit. If the perturbation is stronger then the separation between perturbed and unperturbed orbit quickly becomes macroscopic at which point the divergence evolves slower than exponentially.

The extent to which a Langevin equation with white noise can simulate discreteness effects associated with motion in a frozen-N system was tested in two ways: (a) visual comparison of the plots for the dispersions σ_r generated for frozen-N and noisy ensembles, and (b) a comparison of the slopes associated with the growth law for σ_r.

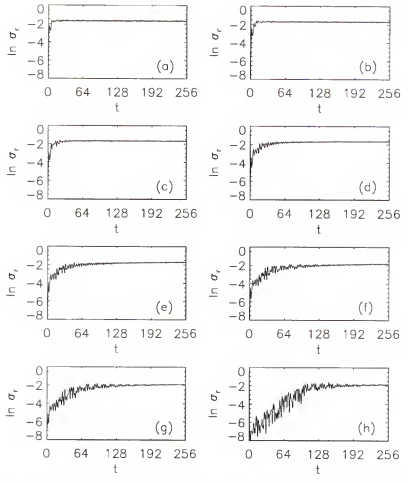

Figure 6.2: The configuration dispersion σ_r associated with an initially localised ensemble of wildly chaotic orbits evolved in the presence of noise of the nonintegrable ellipsoid potential (2.4) for $\Theta = 1.0$ and variable η. (a) $\eta = 10^{-2.0}$. (b) $\eta = 10^{-2.5}$. (c) $\eta = 10^{-3.0}$. (d) $\eta = 10^{-3.5}$. (e) $\eta = 10^{-4.0}$. (f) $\eta = 10^{-4.5}$.(g) $\eta = 10^{-5.0}$. (h) $\eta = 10^{-7.5}$.

It is obvious from Figure 6.1 (compare it to Figure 5.2) that for the Plummer potential there is a significant qualitative (visual) agreement between the plots describing the time evolution of σ_r in the two regimes, frozen-N and 'noisy', at least for $N \geq 10^4$. For very small values of N there are significant differences since the frozen-N σ_r grows considerably more rapidly than the noisy one.

There is also a considerable similarity for the case of chaotic orbits, as is evident from Figure 6.2 (compare it with Figure 5.3) for wildly chaotic orbits and Figure 6.3 (compare it with Figure 5.4) for "sticky" chaotic orbits. Assuming that

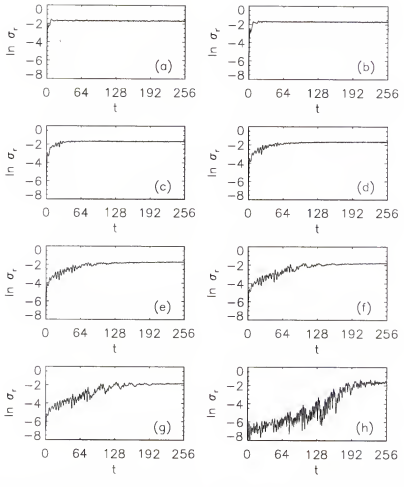

Figure 6.3: The configuration dispersion σ_r associated with an initially localised ensemble of 'sticky' chaotic orbits evolved in the presence of noise of the nonintegrable ellipsoid potential (2.4) for $\Theta = 1.0$ and variable η. (a) $\eta = 10^{-2.0}$. (b) $\eta = 10^{-2.5}$. (c) $\eta = 10^{-3.0}$. (d) $\eta = 10^{-3.5}$. (e) $\eta = 10^{-4.0}$. (f) $\eta = 10^{-4.5}$. (g) $\eta = 10^{-5.0}$. (h) $\eta = 10^{-7.5}$.

the correspondence between N and η can be extrapolated for larger N it follows that the particle number required for chaotic orbits in order for the discreteness effects to become unimportant is as large as $N \sim 10^8$.

The exact association between values of N and values of η can be accomplished if we notice that the noisy dispersions are also well fit by a $t^{1/2}$ growth law where, however,

$$t_G = Bt_D/\eta, \tag{6.3}$$

with B a constant of order unity. A comparison of eqs. 6.3 and 5.4 implies a natural identification:

$$\log_{10} \eta = \mathcal{A} - \log_{10} N, \tag{6.4}$$

with $\mathcal{A}$ yet another constant. For the ellipsoid potential, the best fit $\mathcal{A} = 0.0 \pm 0.1$. For the Plummer potential $\mathcal{A} = 0.6 \pm 0.1$. The identification between Figures 5.2 and 6.1 was effected assuming $\mathcal{A} = 0.5$. The extent to which the growth rates for frozen-N and noisy orbits can be related by the simple relation 6.4 can be gauged from Figure 6.4, which superimpose plots of $t_G(N)$ and $t_G(\eta)$ for the Plummer and ellispoid potentials, with N and η related by eq. 6.4.

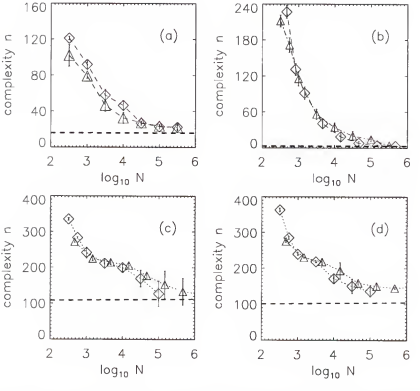

Figure 6.4: The mean complexity n for orbits evolved in the potentials (2.3), (2.1), and (2.6), considering both frozen-N orbits with variable N (diamonds) and smooth orbits perturbed by noise with $\Theta = 1.0$ and variable η (triangles). η was related to N by the relation $\eta = e^{\mathcal{A}}/N$, with $\mathcal{A}$ determined as described in the text. The dashed horizontal line exhibits the mean complexity of orbits with the same initial conditions evolved in the smooth potential in the absence of noise. (a) Regular orbits in the Plummer potential. (b) Regular orbits in the three-dimensional harmonic oscillator potential. (c) Wildly chaotic orbits in the three-dimensional harmonic oscillator plus perturbation potential. (d) 'Sticky' chaotic orbits in the ellipsoid plus black hole potential.

CHAPTER 7
NUMERICAL ESTIMATION OF SMOOTH LYAPUNOV EXPONENTS

There is one question left ananswered and it is important we try to investigate it. I have mentioned that the Lyapunov exponents computed for the frozen-N distributions have values much larger than the values they have for the corresponding smooth potential integration. The Lyapunov exponents χ_N associated with frozen-N descriptions characterize the divergence associated with microscopic effects, while the Lyapunov exponents χ_S computed for orbits evolving in smooth potentials are associated with the macroscopic effect of the smooth potential. For a frozen-N orbit the contribution of the smooth potential Lyapunov exponent is hidden under the significantly larger contribution of the N-body Lyapunov exponent. The question then is the following: is it possible by any method to extract the smooth Lyapunov exponent from the evolution of an orbit in a frozen-N environment?

The answer to this question seems to be "yes" but only when N is large enough (at least $10^{4.5}$). The key to this answer is given by the careful inspection of the early evolution of the divergence between two orbits starting from very close distance in the phase space and evolving in the same frozen-N environment. Then different behaviour is met depending on whether the orbit corresponds to a regular or a chaotic one in the smooth environment.

If the corresponding orbit in the smooth regime is regular then the two orbits diverge initially exponentially at a rate $\Lambda \sim \chi_N$ and this divergence quickly saturates once the separation between the orbits has become large compared to the

typical distance between the point masses. Then this initial exponential divergence is replaced by a power law divergence which proceeds on time scale $t_G \propto N^{1/2} t_D$.

If the corresponding orbit in the smooth potential is chaotic then again the initial divergence is exponential at a rate $\Lambda \sim \chi_N$, but then this is replaced by an exponential divergence at a rate $\Lambda \sim \chi_S$, and eventually it ends up to a power law divergence which proceeds on time scale $t_G \propto (\ln N) t_D$.

These statements can become clearer if one tracks the evolution of the seperation:

$$\delta r(t) = |\mathbf{r_1} - \mathbf{r_2}| \tag{7.1}$$

and then in order to compute the average divergence for a phase space region we can select an ensemble of initial conditions from that region evolve them and then compute the quantity:

$$\langle \delta r \rangle = \frac{1}{n} \sum_{i=1}^{n} \delta r_i \tag{7.2}$$

Figure 7.1 exhibits the results of such computation for an ensemble of 100 orbits generated from regular initial conditions in the Plummer potential. Figure 7.2 exhibits the results for chaotic initial conditions in the three-dimensional plus perturbation potential. The N for the frozen-N environments varies from $10^{4.5}$ to 10^6, and the initial conditions sampled a phase space region of size $\Delta r \sim \Delta v \sim 10^{-3}$. The different behaviour for regular and chaotic orbits is obvious. After the initial exponential divergence associated with the microchaos the chaotic orbits move to another exponential divergence of which the exponent is associated with the macrochaos, while the regular orbits move to a power law regime.

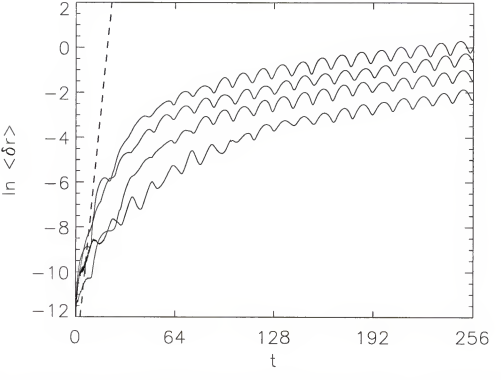

Figure 7.1: The mean spatial separation between orbits generated in the frozen-N analogue of the Plummer potential, from initial conditions seperated in configuration space by a distance $\delta r(0) = 10^{-5}$. The four curves correspond (from top to bottom) to $N = 10^{4.5}$, $N = 10^5$, $N = 10^{5.5}$, $N = 10^6$. Each curve was generated by averaging over 100 pairs of initial conditions.

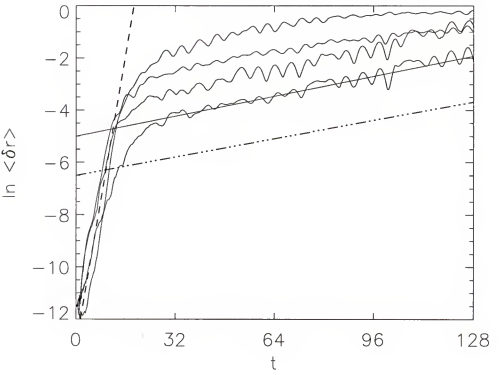

Figure 7.2: The mean spatial separation between orbits generated in the frozen-N analogue of the three-dimensional plus perturbation potential, from initial conditions seperated in configuration space by a distance $\delta r(0) = 10^{-5}$. The four curves correspond (from top to bottom) to $N = 10^{4.5}$, $N = 10^{5}$, $N = 10^{5.5}$, $N = 10^{6}$. The solid curve corresponds to a slope of 0.022, generated as a least squares fit. The triple dot-dashed line has a slope 0.026, equal to the mean value of the smooth Lyapunov exponent. The dashed line has a slope 0.75, equal to the mean value of the N-body Lyapunov exponent χ_N. Each curve was generated by averaging over 100 pairs of initial conditions.

CHAPTER 8
CONCLUSIONS

The purpose of this thesis was to understand the validity of the continuum limit associated with the smooth potential description of N-body systems and to characterize it quantitatively as well as qualitatively.

Lyapunov exponents associated with motion of orbits in frozen-N configurations have, in general, values that are significantly larger than the value they have for the same initial conditions evolved in smooth potential environments. It is clear that the Lyapunov exponents computed numerically for orbits that evolve in smooth potentials are associated with the form of the bulk potential. When the potential is integrable these Lyapunov exponents are zero but when the potential is nonintegrable they have some positive value. For the case of nonintegrable potentials this positive value is associated with the macroscopic chaos, or macrochaos, generated by the potential as a whole. The orbits evolving in frozen-N environments are characterized by Lyapunov exponents that are associated mainly with the discreteness effects, i.e. they are generated by a microscopic chaos, or microchaos. This does not mean that in the case of frozen-N configurations associated with nonintegrable potentials there is no contribution to the destabilization of the orbit because of the action of the potential as a whole (macrochaos). It is simply that this contribution is small compared to the contribution by the discreteness effects.

Probably the most striking result was the fact that the Lyapunov exponents of orbits evolved in frozen-N configurations do not decrease as N increases, even though their power spectrum becomes simpler and approaches the form it has when

the orbit is evolved in the smooth potential. This means that in the case of motion in an N-body system that corresponds to an integrable potential in the continuum limit, for very large N an orbit will visually look completely regular, but it will still be characterized by a large Lyapunov exponent, i.e. it will be chaotic in the sense of sensitivity on initial conditions. To this extent Lyapunov exponents fail to describe the regularity or chaos in a visual sense, since χ does not decrease even when the 'range' of chaos gets shorter.

There is however a theoretical argument that can explain the inconsistency. Since in the frozen-N environments chaos is generated by discreteness effects, i.e. the random interactions between a test paricle and a collection of field particles one can use the tidal effects associated with a pair of particles separated by a distance comparable to the typical interparticle separation in order to estimate the time necessary for the growth of an initial perturbation. The tidal acceleration will scale as:

$$\delta\ddot{\mathbf{r}} = (\delta\mathbf{r}\cdot\nabla)\mathbf{a} \sim \frac{Gm}{r^3}\delta\mathbf{r}, \tag{8.1}$$

where m is the particle mass and r the separation. Since

$$r \sim n^{-1/3} \sim N^{-1/3}R_{sys} \tag{8.2}$$

with n the characteristic number density and R_{sys} the size of the system, it follows that the time scale associated with the growth of an initial perturbation will be:

$$t_* \sim 1/\sqrt{G\rho}. \tag{8.3}$$

which is comparable to the dynamical time t_D and independent of N. As N increases the individual mass ($m = M/N$) and the cube of the separation between particles, n^{-1}, both decrease as N^{-1} so that the ratio does not depend on N.

The second measure of quantification of chaos, that is the complexity of the power spectrum of the orbits, agreed completely with the visual qualitative description of the orbit. Orbits evolving in smooth integrable potentials are characterized by very simple power spectra, where all the power is concentrated in a small number of frequencies. The evolution in the corresponding frozen-N configurations gives a more complicated power spectrum for small N as well as a more complicated orbit in a visual sense. However as N increases the orbit and the power spectrum gradually become less complicated and they approach the form they have in the continuum limit, i.e. the smooth case.

For the nonintegrable potentials the investigation is a little more difficult because the power spectrum of chaotic orbits have a very complex visual appearance and a very complex power spectrum when they evolve in the smooth potential. In the frozen-N systems, for small N the power spectrum becomes even more complex. However as N increases the visual appearance and power spectra gradually approach the form they have in the continuum limit case, in exactly the same way that regular orbits do.

One fundamental question to be answered was how an orbit starting from some initial condition and evolving in a smooth potential environment, diverges from an orbit starting from the same initial condition but evolving in a frozen-N analogue of the smooth potential. For position and velocity variables the evolution of this divergence was in general linear in time and the growth time associated with this evolution was $\propto \sqrt{N}$ for the regular potentials and $\propto \ln N$ for the chaotic ones. This means that regular orbits remain close to the smooth characteristic for time much longer than do the chaotic orbits.

In terms of quantities like angular momentum that are invariant in the smooth potential, the divergence of frozen-N orbits from the smooth characteristic is given as $(t/t_J)^{1/2}$ with $t_J \sim \sqrt{N}$. This characterizes a diffusive process which suggests

that discretensess effects can be modeled as white Gaussian noise in the context of a Langevin or Fokker-Planck description.

For both regular and chaotic systems phase mixing is more efficient for small N configurations than for the corresponding smooth potential case. As N increases the phase mixing evolution resembles more and more the phase mixing evolution in the smooth potential.

Transitions between regular and chaotic orbits can and do arise in frozen-N configurations, an effect which is of course impossible for the smooth characteristics. These transitions are more common and happen more easily for small N. As N increases and approaches the continuum limit they become more and more difficult. Transitions between sticky and wildly chaotic orbits can happen in the smooth case but they happen on a much shorter time scale for small N in an N-body environment.

For comparatively large N discreteness effects can be mimicked by energy-conserving white noise with amplitude $\eta \propto 1/N$. This definitely agrees with the expectation that discreteness effects can be modeled as a sequence of incoherent binary encounters. The results of simulations in frozen-N environments and in 'noisy' configurations agreed in statistical sense. Therefore we conclude that noise can be used to model both bulk statistical properties of orbit ensembles and qualitative properties of individual orbits. This means that the results of experiments based on the Langevin description (which are computationally 'cheap') can be trusted at least as first approximation, to give important information about the effects of graininess.

However it is clear that modeling discretness effects using the Langevin description is not absolutely satisfactory. For small N it fails to give similar results with the N-body description. Moreover the N-body Lyapunov exponents cannot be correctly computed in such a regime. Other forms of noise, instead of white

noise, can be more suitable for better results. This is a question to be addressed by further research on the subject.

The final conclusion of this thesis is that at least in terms of macroscopic properties the continuum limit is valid for $N \to \infty$. However convergence towards this limit is substantially slower for density distributions that correspond in the continuum limit to nonintegrable potentials and admit a significant measure of chaotic orbits, than for density distributions that correspond in the continuum limit to integrable potentials.

REFERENCES

[1] R. H. Miller, Astrophys. J. **140**, 250 (1964).

[2] H. E. Kandrup, Physica A **169**, 73 (1989).

[3] J. Goodman, D. Heggie, and P. Hut, Astrophys. J. **415**, 715 (1993).

[4] R. W. Hockney, J. W. Eastwood, *Computer Simulation Using Particles* (Philadelphia : A. Hilger, 1988).

[5] J. Binney and S. Tremaine, *Galactic Dynamics* (Princeton University Press, Princeton, 1987).

[6] H. E. Kandrup and H. Smith, Astrophys. J. **374**, 255 (1991).

[7] M. Tabor, *Chaos and Integrability in Nonlinear Dynamics* (Wiley, New York, 1989).

[8] A. J. Lichtenberg and M. A. Lieberman, *Regular and Chaotic Dynamics* (Springer, Berlin, 1992).

[9] G. Bennetin, L. Galgani, A. Giorgilli, and J. M. Strelcyn, Meccanica, **15**, 9 (1980)

[10] M. E. Mahon, R. A. Abernathy, O. B. Bradley, H. E. Kandrup, Mon. Not. R. astr. Soc. **275**, 443 (1995).

[11] H. E. Kandrup, Mon. Not. R. astr. Soc. **301**, 960 (1998).

[12] H. E. Kandrup, I. V. Pogorelov, and I. V. Sideris, Mon. Not. R. astr. Soc. **311**, 719 (2000).

[13] C. L. Bohn, H. E. Kandrup, and R. A. Kishek, *Proceedings of Snowmass 2001*, ed. C. M. Sazama eConf C01/06/30, M302 (2001).

[14] S. Chandrasekhar, Rev. Mod. Phys. **15**, 1 (1943).

[15] S. Chandrasekgar, *Principles of Stellar Dynamics* (University of Chicago, Chicago, 1943).

[16] H. E. Kandrup, M. E. Mahon, and H. Smith, Astrophys. J. **428**, 458 (1994).

[17] S. J. Aarseth, M. Hénon, and R. Wielen, Astron. Astrophys. **37**, 183 (1974).

[18] H. E. Kandrup, Phys. Reports, **63**, 1 (1980).

[19] C. Siopis and H. E. Kandrup, Mon. Not. Roy. Astro. Soc. **319**, 43 (2000).

[20] H. E. Kandrup, B. L. Eckstein, and B. O. Bradley, Astron. Astrophys. **320**, 65 (1997).

[21] K. P. Rauch and S. Tremaine, New. Astron. **1**, 149 (1996).

[22] M. Valluri and D. Merritt, in *The Chaotic Universe*, ed. R. Ruffini and V. G. Gurzadyan (World Scientific, New York, 1999).

[23] S. Chandrasekhar, Rev. Mod. Phys. **15**, 1 (1943).

[24] H. E. Kandrup and I. V. Sideris, Phys. Rev. **E 64**, 056209.

[25] M. Valluri and D. Merritt, in *The Chaotic Universe*, edited by R. Ruffini and V. G. Gurzadyan (World Scientific, New York, 1999).

[26] S. Habib, H. E. Kandrup, and M. E. Mahon, Astrophys. J. **480**, 155 (1997).

[27] H. E. Kandrup and S. Novotny, Phys. Rev. **E**, submitted.

[28] H. E. Kandrup, B. L. Eckstein, and B. O. Bradley, Astron. Astrophys. **320**, 65 (1997).

[29] G. Bertin, *Dynamics of Galaxies* (Cambridge University Press, Cambridge, 2000).

[30] H. E. Kandrup and I. V. Sideris, Celestial Mechanics, **82**, 61 (2002).

[31] W. Dehnen, Mon. Not. R. astr. Soc. **265**, 250 (1993).

[32] D. Merritt and T. Fridman, Astrophys. J. **460**, 136 (1996).

[33] C. Siopis and H. E. Kandrup, Mon. Not. R. astr. Soc. **319**, 43 (2000).

[34] C. Siopis, Ph. D. University of Florida, dissertation, 1998.

[35] N. G. van Kampen, *Stochastic Processes in Physics and Chemistry* (North Holland, Amsterdam, 1981).

[36] A. Griner, W. Strittmatter, and J. Honerkamp, J. Stat. Phys. **51**, 95 (1989).

[37] C. Siopis, B. L. Eckstein, and H. E. Kandrup, Ann N. Y. Acad. Sci. **867**, 41 (1998).

[38] C. L. Bohn and J. R. Delayen, Phys. Rev. **E 50**, 1516 (1994).

[39] W. H. Press, S. A. Teukolsky, W. T. Vetterling, B. P. Flannery, *Numerical Recipes in C* (Cambridge University Press, Cambridge, 1995)

[40] Myron Lecar, *Gravitational N-body problem; proceedings of IAU colloquium no. 10*, Cambridge, England, August 12-15, 1970.

[41] M.E. Standish Jr., K. Aksnes, Astrophys. J. **158**, 519 (1969).

[42] I. V. Sideris and H. E. Kandrup, Phys. Rev. **E**, in press.

[43] H. E. Kandrup and I. V. Sideris, Astrophys. J., submitted.

BIOGRAPHICAL SKETCH

I was born in a small city in Greece thirty one years ago but a little bit later my family moved to Athens. This is where I stayed till I was eighteen but then I had to move the Thessaloniki for my studies. Five years later I graduated with a degree in Physics and many dreams for a future career as an astronomer. Back then I had not realised, but it is clear to me now, how important were those years in Greece. Living and growing up in an environment with such rich geography built in me the amazing structure we call imagination. Living in a place with rich historical background opened my mind to love for ideas, books, and intelligent discussions.

Then I came to the United States. I stayed in New York for about two years, I interacted with people from all over the world in a huge ferment, and that gave me the opportunity to understand better the human psychology by observing the human behaviour. In 1995 I moved to Gainesville and I started my studies. I was admitted to the Astronomy department in 1996 and two years later I started working with Dr. Kandrup in galactic dynamics, theory of chaos, and stochastic processes. Through his guidance and a lot of personal effort, I acquired a significant background in computer programming and simulations. I will soon move to Illinois where I will work in an accelerator dynamics division as a simulator.

I certify that I have read this study and that in my opinion it conforms to acceptable standards of scholarly presentation and is fully adequate, in scope and quality, as a dissertation for the degree of Doctor of Philosophy.

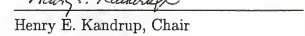

Henry E. Kandrup, Chair
Professor of Astronomy

I certify that I have read this study and that in my opinion it conforms to acceptable standards of scholarly presentation and is fully adequate, in scope and quality, as a dissertation for the degree of Doctor of Philosophy.

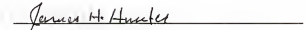

James H. Hunter
Professor of Astronomy

I certify that I have read this study and that in my opinion it conforms to acceptable standards of scholarly presentation and is fully adequate, in scope and quality, as a dissertation for the degree of Doctor of Philosophy.

Haywood C. Smith
Associate Professor of Astronomy

I certify that I have read this study and that in my opinion it conforms to acceptable standards of scholarly presentation and is fully adequate, in scope and quality, as a dissertation for the degree of Doctor of Philosophy.

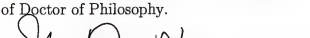

James W. Dufty
Professor of Physics

I certify that I have read this study and that in my opinion it conforms to acceptable standards of scholarly presentation and is fully adequate, in scope and quality, as a dissertation for the degree of Doctor of Philosophy.

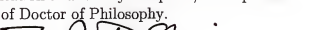

Zoran Pop-Stojanovic
Professor of Mathematics

This dissertation was submitted to the Graduate Faculty of the College of Liberal Arts and Sciences and to the Graduate School and was accepted as partial fulfillment of the requirements for the degree of Doctor of Philosophy.

August 2002

Dean, Graduate School